Few-Body Systems 9, 165–194 (1990)

Few-Body Systems

Investigation of the ^{3}He($\vec{d}$, p)^{4}He Reaction Between 1 and 13 MeV

M. Bittcher, W. Grüebler, V. König[1], P. A. Schmelzbach[2], B. Vuaridel[3], and J. Ulbricht[4]

Institute for Intermediate-Energy Physics, ETH Hönggerberg, CH-8093 Zürich, Switzerland

Abstract. High-precision measurements of the cross section, the vector analyzing power iT_{11} and the three tensor-analyzing powers T_{20}, T_{21}, and T_{22} of the ^{3}He(d, p)^{4}He reaction have been performed in the energy range between 1.0 and 13.0 MeV in steps of 1 or 2 MeV. Angular distributions of the cross section have been obtained between 22.5° and 157.5° in the laboratory system. The polarization observables have been measured between 10° and 170°.

1 Introduction

The investigation of the nucleon-nucleon (N-N) interaction and its application to few-nucleon systems are fundamental tasks in nuclear physics. Theoretical models use as testing grounds preferably nuclear reactions involving few-nucleon systems. In general, differential cross-section data mainly reflect the features of the central force, while from polarization observables mostly the details of the spindependent interactions are extracted. At low energy polarization effects are very small in N-N scattering. However, in few-nucleon systems it is found that polarization observables can increase by one to two orders of magnitude. The complexity of the structure of few-nucleon systems with $A > 3$ is increased by the existence of resonances. The possibility of measuring polarization observables to a very high precision allows one to detect in an analysis of these data also tiny effects in the underlying interactions.

In the past, the five-nucleon systems ^{5}He and ^{5}Li have been the subject of many experimental and theoretical studies [1–10]. Basically there exist only two configurations with a two-cluster structure, the 4 + 1 and the 3 + 2 configuration. Since

[1] *Present address*: Perinatalphysiologisches Labor, Frauenklinik USZ, CH-8091 Zürich, Switzerland

[2] *Present address*: Paul-Scherrer-Institut, CH-5232 Villigen PSI, Switzerland

[3] *Present address*: Randall Laboratory of Physics, The University of Michigan, Ann Arbor, MI 48109, and Brookhaven National Laboratory, Box 633, Upton, NY 11973, USA

[4] *Present address*: Institute for High-Energy Physics, ETH Hönggerberg, CH-8093 Zürich, Switzerland

the simplest 4-nucleon cluster, the α-particle, is very stable and also the 3-nucleon systems have a high binding energy the most probable three-cluster structure has a $3 + 1 + 1$ configuration. The $4 + 1$ configuration has been extensively investigated by elastic p-α scattering [1] up to fairly high excitation energy and partly by n-α scattering [1]. The phase-shift analyses of these data have successfully clarified the corresponding p-α structure in this nucleus. Compared with these results the d-^{3}He clustering is not so well known, since the $3 + 2$ configuration was studied systematically by the d-^{3}He elastic scattering only for incident deuteron energies smaller than about 14 MeV [11, 12]. The configurations of the five-nucleon system at higher excitation energy can be investigated effectively by the ^{3}He$(d, p)^4$He reaction. This reaction also has the advantage that the tensor interaction plays an important role due to the deuteron in the incident channel. Information about the processes and configurations involved can be gained not only by the differential cross section and the vector polarization but also by the tensor polarization observables.

The d-^{3}He entrance channel leads to a highly excited ^{5}Li nucleus. This entrance configuration of the compound nucleus transforms into a $^4\text{He} + p$ exit-channel configuration, which releases a high amount of energy. The Q-value of the ^{3}He$(d, p)^4$He reaction is + 18.35 MeV. The theoretical treatment of this reaction is facilitated, since neither the ^{3}He nor the ^{2}H cluster in the entrance channel have excited states and therefore no internal excitation of these single clusters in this configuration has to be taken into account. In the exit channel only highly excited states in ^{4}He exist, which have a weak excitation probability. Therefore model calculations are relatively simple and can concentrate on the aspects of the more interesting N-N interactions in a few-nucleon system.

The ^{3}He$(d, p)^4$He reaction is also known as an analyzer reaction for deuteron polarimeters, since not only the vector-analyzing power but also all three tensor-analyzing powers have high values over a large energy range. They all are smooth and therefore allow for thick targets in a polarimeter, such that the deuteron polarization components can be determined accurately even in double-scattering experiments.

For these reasons we have measured the vector- and tensor-analyzing powers as well as the cross section of the ^{3}He$(d, p)^4$He reaction in the energy range between 1 and 13 MeV in small energy steps. Nearly complete angular distributions of these observables have been determined. The new data have a much higher precision than previous results [13], due to better statistical accuracy as well as better absolute calibration.

2 Experimental Method

2.1 Measurement of the Differential Cross Section $\sigma(\theta)$

The measurement of the cross section was performed with an unpolarized beam. The cross section $\sigma(\theta)$ is given by the ratio of the number of emitted protons N_p to the number of incident deuterons N_d, the target density n_t, and a geometrical factor $G/\sin\theta$,

$$\sigma = \frac{N_p}{N_d n_t} \cdot \frac{\sin\theta}{G} . \tag{1}$$

The quantity G was calculated for our detector system via the formalism of Silverstein [14]. The number of protons N_p was determined from the spectra of detectors symmetrically positioned on the left and the right. The number of incident deuterons N_d was measured in the Faraday cup, which was connected to a current integrator. The target density n_t was determined by the measurement of the pressure and temperature of the gas target.

2.2 *Measurement of the Analyzing Powers*

In the helicity frame of an atomic beam-type polarized ion source the polarization of the produced deuterons is described most conveniently by the vector polarization $\hat{t}_{10}$ and the tensor polarization $\hat{t}_{20}$. These source parameters refer to the direction of the magnetic field in the ionizer of the source, which is parallel to the momentum of the extracted beam. A nuclear reaction induced by an accelerated beam can be described in a target coordinate system as shown in Fig. 1. Here the z-axis points along the incident-beam momentum $\mathbf{k}_{in}$, y is along the normal to the scattering plane $\mathbf{n} = \mathbf{k}_{in} \times \mathbf{k}_{out}$. The spin-alignment axis $\mathbf{s}$ makes an angle α with $\mathbf{k}_{in}$ and the projection of $\mathbf{s}$ onto the xy-plane has an angle β with respect to $\mathbf{n}$.

In this target coordinate system (cf. Fig. 1) the spin-dependent cross section for a nuclear reaction with polarized deuterons is given by

$$\sigma(\Theta) = \sigma_0(\Theta) \cdot \left\{1 + \sqrt{2} \sin\alpha \cdot \cos\beta \cdot \hat{t}_{10} \cdot iT_{11} + \frac{1}{2}(3\cos^2\alpha - 1) \cdot \hat{t}_{20} \cdot T_{20} + \sqrt{\frac{3}{2}} \sin 2\alpha \cdot \sin\beta \cdot \hat{t}_{20} \cdot T_{21} - \sqrt{\frac{3}{2}} \sin^2\alpha \cdot \cos 2\beta \cdot \hat{t}_{20} \cdot T_{22}\right\}, \quad (2)$$

where the analyzing powers T_{kq} are denoted after the Madison Convention [15]. In the present work the four analyzing powers T_{kq} are measured in four separate runs where the direction of $\mathbf{s}$ is chosen by the angles α and β such that the experimental

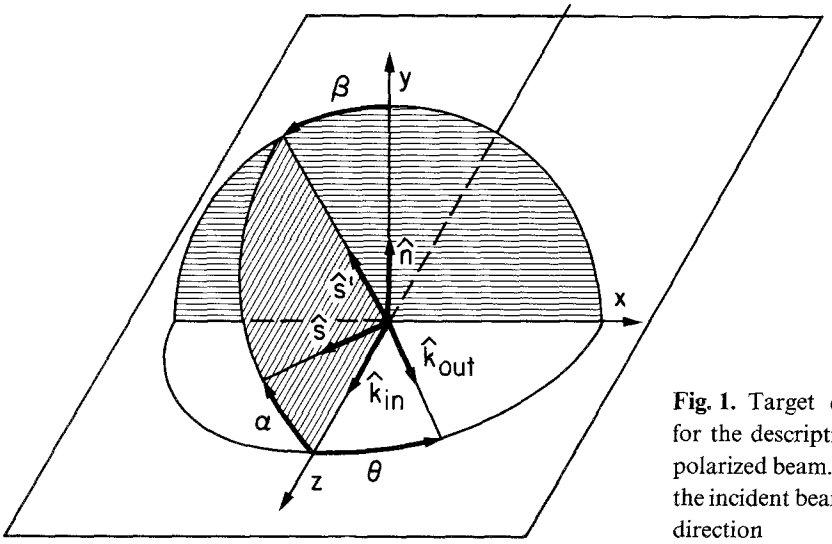

Fig. 1. Target coordinate system for the description of the incident polarized beam. The momentum of the incident beam $\mathbf{k}_{in}$ is along the z-direction

errors are minimized. These spin angles could be set to the desired values by a Wien filter, which can be rotated around the beam axis, mounted between the polarized ion source and the tandem accelerator.

The three rf-transitions in the neutral atomic beam of the source allow to change between positive and negative values of the beam polarization. In Table 1 the three rf-transition configurations are shown. Switching between configuration *b* and *c* changes the sign of the source parameters $\hat{t}_{10}$ and $\hat{t}_{20}$ and switching between *d* and *e* changes the sign of the purely vector-polarized beam. The sign changes which occured about every second were controlled by the target current integrator collecting a preset amount of charge for every polarization state. In the computer the spectra for both polarization states were stored separately. The rf-transitions were tuned carefully in order to obtain the same absolute value of the polarization for both signs. For each scattering angle Θ a pair of detectors was mounted in the horizontal plane, one on the left-hand side with a spin-rotation angle β and the other on the right-hand side at the same angle Θ and the spin-rotation angle $\beta + \pi$. From these two detectors and the negative and positive beam polarization four counting rates N_L^+, N_L^-, N_R^+, N_R^- are obtained, from which the ratios L and R—for the left and right detectors, respectively—can be calculated, both being independent of the solid angles,

$$L = \frac{N_L^+ - N_L^-}{N_L^+ + N_L^-} = +\sqrt{2}\sin\alpha\cdot\cos\beta\cdot\hat{t}_{10}\cdot iT_{11} + \frac{1}{2}(3\cos^2\alpha - 1)\cdot\hat{t}_{20}\cdot T_{20} + \sqrt{\frac{3}{2}}\sin 2\alpha\cdot\sin\beta\cdot\hat{t}_{20}\cdot T_{21} - \sqrt{\frac{3}{2}}\sin^2\alpha\cdot\cos 2\beta\cdot\hat{t}_{20}\cdot T_{22},$$

$$R = \frac{N_R^+ - N_R^-}{N_R^+ + N_R^-} = -\sqrt{2}\sin\alpha\cdot\cos\beta\cdot\hat{t}_{10}\cdot iT_{11} + \frac{1}{2}(3\cos^2\alpha - 1)\cdot\hat{t}_{20}\cdot T_{20} - \sqrt{\frac{3}{2}}\sin 2\alpha\cdot\sin\beta\cdot\hat{t}_{20}\cdot T_{21} - \sqrt{\frac{3}{2}}\sin^2\alpha\cdot\cos 2\beta\cdot\hat{t}_{20}\cdot T_{22}. \quad (3)$$

From these ratios one can determine the sum

$$\frac{L+R}{2} = \frac{1}{2}(3\cos^2\alpha - 1)\cdot\hat{t}_{20}\cdot T_{20} - \sqrt{\frac{3}{2}}\sin^2\alpha\cdot\cos 2\beta\cdot\hat{t}_{20}\cdot T_{22}, \quad (4)$$

which depends only on the even analyzing powers T_{20} and T_{22}.

For $\alpha = 0°$ the term with T_{22} vanishes and for $\alpha = 90°$ and $\beta = 0°$ or $90°$ this term will reach its maximum.

Table 1. Configuration of rf-transitions

	$2 \to 6$	$3 \to 5$	Weak field	$\hat{t}_{10}$	$\hat{t}_{20}$
a	Off	Off	Off	0	0
b	Off	On	On	$-1/\sqrt{6}$	$+1/\sqrt{2}$
c	Off	On	Off	$+1/\sqrt{6}$	$-1/\sqrt{2}$
d	On	On	Off	$+\sqrt{2/3}$	0
e	Off	Off	On	$-\sqrt{2/3}$	0

The difference

$$\frac{L-R}{2} = \sqrt{2}\cdot\sin\alpha\cdot\cos\beta\cdot\hat{t}_{10}\cdot iT_{11} + \sqrt{\frac{3}{2}}\sin 2\alpha\cdot\sin\beta\cdot\hat{t}_{20}\cdot T_{21} \tag{5}$$

depends only on the odd analyzing powers T_{21} and iT_{11}.

For $\beta = 90°$ the term with iT_{11} will vanish and the term with T_{21} will reach the maximum for $\alpha = 45°$. On the other hand the term with iT_{11} will have the maximum value for $\beta = 0°$ and $\alpha = 90°$.

From these considerations it is concluded that the optimal choice of α and β for determining all four analyzing powers with the aid of Eqs. (4) and (5) is

$$\begin{aligned}
&\alpha = 0°: && T_{20} = \frac{1}{\hat{t}_{20}}\cdot\frac{L+R}{2},\\
&\alpha = 90°,\ \beta = 90°: && T_{22} = \frac{1}{\sqrt{\frac{3}{2}}\hat{t}_{20}}\cdot\frac{L+R}{2} + \frac{1}{\sqrt{6}}\cdot T_{20} \quad \text{(with known } T_{20}),\\
&\alpha = 45°,\ \beta = 90°: && T_{21} = \frac{1}{\sqrt{\frac{3}{2}}\hat{t}_{20}}\cdot\frac{L-R}{2},\\
&\alpha = 90°,\ \beta = 0°: && iT_{11} = \frac{1}{\sqrt{2}\hat{t}_{10}}\cdot\frac{L-R}{2} \quad \text{(with purely vector-polarized beam).}
\end{aligned} \tag{6}$$

If the spin-direction angles α and β deviate from the correct values by $\Delta\alpha$ and $\Delta\beta$, the following errors for the T_{kq} are obtained,

$$\begin{aligned}
\Delta T_{20} &= \frac{3}{2}\Delta\alpha^2\cdot T_{20} + \sqrt{\frac{3}{2}}\cos 2\beta\cdot\Delta\alpha^2\cdot T_{22},\\
\Delta T_{22} &= \left(\frac{1}{2}\Delta\alpha^2 + 2\Delta\beta^2\right)\cdot T_{22} - \sqrt{\frac{3}{2}}\Delta\alpha^2\cdot T_{20},\\
\Delta T_{21} &= \left(2\Delta\alpha^2 + \frac{1}{2}\Delta\beta^2\right)\cdot T_{21} + \frac{\sqrt{2}}{3}(\Delta\beta + \Delta\alpha\,\Delta\beta)\cdot iT_{11},\\
\Delta iT_{11} &= \frac{1}{2}(\Delta\alpha^2 + \Delta\beta^2)\cdot iT_{11}.
\end{aligned} \tag{7}$$

All terms in $\Delta\alpha$ are quadratic and therefore in the worst case, i.e., for all T_{kq} maximal, an error of about 0.0025 is obtained for a value of $\Delta\alpha = 2°$. This means that a determination of $\alpha \pm 2°$ is sufficient for an accuracy in T_{kq} of magnitude 0.0025. The same is true with respect to the angle β, except for T_{21}: In this case there exists a term with $\Delta\beta\cdot iT_{11}$, which is only linear in $\Delta\beta$, and therefore requires $\Delta\beta < 1°$ for an error smaller than 0.0025 in T_{21}.

In conclusion the advantages of this method are the following:

(a) Since only two detectors in one plane are used, it is easier to measure at extreme forward and backward angles or to measure more scattering angles Θ simultaneously than with a device with four detectors in two planes.
(b) The measurement is independent of the ratio of the solid angles of both detectors.

(c) For an accuracy of T_{kq} of the order of 0.0025, a determination of the spin-direction angles α and β to only $\pm 2°$ is sufficient. However, the same accuracy for T_{21} requires an accuracy of β better than $\pm 1°$.
(d) The statistical accuracy of the measured T_{kq} is better for a measurement changing the sign of the beam polarization than for a measurement comparing only the polarized and unpolarized beams.

3 Experimental Arrangement

3.1 Polarized Beam

The measurements of the cross section and the analyzing powers were carried out with the polarized deuteron beam from the ETH EN tandem accelerator. The polarized ion source [16] was based on the atomic beam method with rf-transitions in the neutral beam followed by an ionizer and a charge exchanger. A beam-rotation device (Wien filter) oriented the spin in the direction that was optimal for the determination of the analyzing power under consideration (cf. Sect. 2). After acceleration by the tandem accelerator the beam was analyzed in a 90° magnet, then deflected by a 15° switching magnet, finally sent through two tantalum collimators 5 and 3 mm in diameter spaced 30 cm apart. The first collimator consisted of four sectors, where the beam intensity hitting the sectors could be measured. The final collimator was cut in half (left and right) and the two segments were isolated from ground and from each other. This arrangement enabled the control of the focussing of the beam entering the ^{3}He gas target.

3.2 Scattering Chamber

The measurement of the observables was performed in a scattering chamber 75 cm in diameter. The polarized beam entered through the collimator system into the ^{3}He gas target and was collected in a Faraday cup equipped with an electrostatic suppressor electrode. The emitted protons were collimated by a rectangular-slit system with antiscattering baffles placed between the defining apertures. The first slits were 2 mm wide, at a distance of 48 mm from the target center, the second slits were located on a radius of 244 mm. Their widths were 4 mm, the heights were nominally 38 mm, which could be reduced for forward angles. These slit apertures were machined to within 0.02 mm of the nominal values. The angular resolution is $\Delta\Theta = \pm 0.5°$ (FWHM). A pair of two slit systems, each having four detector positions spaced by 5°, was used in the present experiment. The slit systems were mounted on two turntables located symmetrically around the direction of the incident polarized beam. Thus the 4 detector pairs covered an angular range of 15° on the left- and right-hand sides, what allowed the measurement of four asymmetries simultaneously. A total angular range between 10° and 170° could be measured with this setup. The turntables could be adjusted remotely controlled to the desired position to within 0.1°.

3.3 Gas Target

The gas target was a cylinder 16 mm in diameter having a beam-entrance window 5 mm in diameter and an exit aperture 6 mm high ranging from $-135°$ to $+135°$.

Rotation of the target by 180° opened the corresponding backward angular range. The entrance and exit windows were made of 2.5 μm thick Havar foils glued in place by means of an epoxy resin. The target contained 1.5 bar ^3He gas with a purity of 99.9%.

3.4 Detector System

The emitted protons from the reaction were measured by silicon-surface barrier detectors with a sensitive area of 10 × 40 mm. These detectors were 1 mm thick stopping protons of up to 12 MeV completely. Aluminium absorbers were used in order to reduce the energy of the protons from the reaction and to stop other reaction products completely, e.g., the elastically scattered deuterons.

3.5 Beam Polarimeter

The tensor polarization of the deuteron beam was monitored continuously in a polarimeter. This device is based on the $^3He(d, p)^4He$ reaction too. A ^3He gas cell was mounted at the end of the Faraday cup. The emitted protons were measured at an angle of 0° with a circular detector subtending an effective angle $\Delta\Theta \leqslant 1°$. While the deuterons from the primary beam were stopped in the back wall of the gas cell the protons passed through and were detected in a CsI scintillator. For a scattering angle of 0° the polarimeter was only sensitive to the t_{20} component of the beam. The counting rate N in the detector is given by

$$N^{\pm} = N_0[1 \pm t_{20} T_{20}(0°)] = N_0[1 \pm \tfrac{1}{2}(3\cos^2\alpha - 1)\hat{t}_{20} T_{20}(0°)], \tag{8}$$

where N_0 is the counting rate for an unpolarized beam. By switching the beam polarization between + and − values the corresponding counting rates N^+ and N^- of the protons in the polarimeter detector allowed the determination of the value of the beam polarization,

$$\hat{t}_{20} = \left[\frac{1}{2}(3\cos^2\alpha - 1) T_{20}(0°)\right]^{-1} \cdot \frac{N^+ - N^-}{N^+ + N^-}. \tag{9}$$

The analyzing power $T_{20}(0°)$ is smooth over a large energy range and has been determined in refs. [17, 18]. A typical tensor polarization of $\hat{t}_{20} = 0.59$ corresponding to 83% of the theoretical maximum was observed.

The polarization of the vector-polarized beam was determined from the calibration iT_{11} of the $^3He(d, p)^4He$ reaction at 10 MeV [19]. A typical value of the vector polarization is $it_{11} = 0.42$, i.e. 82% of the theoretical maximum.

3.6 Electronics

The signals of the eight silicon detectors were amplified by preamplifiers and spectroscopy amplifiers and passed through an analog multiplexer, ADC, and Camac-buffer into a PDP15 computer. After a preselected charge measured in the current integrator the sign of the beam polarization was changed. This guaranteed that the number of incident deuterons was the same for both polarization states.

For the correction of the deadtime the measurement and the current integrator were stopped during the processing of the signals in the ADC and the computer. The dead time in the ADC was kept below 5%.

The spectra of the single detectors were analyzed on-line. Typically a background of about 1% was observed below the proton peaks, which was approximated by a linear function and subtracted from the total number of counts in the peaks.

4 Results

4.1 Cross Section

New measurements of the differential cross section were performed at $E_d = 1, 2, 12,$ and 13 MeV. These angular distributions were measured between $\theta_{lab} = 22.5$ and 157.5° in steps of 5°. The measurement was carried out partially in overlapping configurations in order to assure the consistency of the results. The results are shown in Figs. 2 and 3 together with earlier cross-section measurements from our laboratory [13] in order to give a survey of the behaviour of this observable as a function of energy. The statistical errors for all results are smaller than 0.7% and therefore smaller than the data points in Figs. 2 and 3. The curves are Legendre-polynomial fits to the data. Numerical values of the new data are given in Table 2. The total cross section $\sigma_{tot}/4\pi$, which is equal to the Legendre-polynomial coefficient $a_{00}(0)$, is shown in Table 3. The normalized higher Legendre-polynomial coefficients $d_{00}(L) = a_{00}(L)/a_{00}(0)$ are given in Table 4.

4.1.1 Systematic Errors

The systematic errors are listed in Table 5. The error in the geometry factor G includes all uncertainties in the dimensions of the slit systems and the diaphragms in front of the detectors. Changes in the beam position result in a change of the solid angle of the slit system. In first approximation this effect cancels out, since both left and right detectors are used for the determination of N_p.

The remaining uncertainty in the cross section is

$$\Delta\sigma/\sigma = (\Delta R/R \sin\theta)^2 , \tag{10}$$

where R is the distance between target and detector. For an estimate of this value in Table 5 an unrealistically large $\Delta R = 0.5$ mm was assumed. As can be seen in Table 5 the resulting uncertainty is still very small. The density of the target was determined by the pressure and temperature of the target. For the uncertainty of the density the corresponding errors in these quantities were taken into account. The purity of the ^{3}He target gas was better than 99.9 mol%. The target volume was flushed several times before the final filling.

From the analysis of the spectra the background was found to be typically 1%. The total uncertainty in the analysis is given in Table 5.

4.1.2 Absolute Calibration

In general the uncertainty in the absolute calibration of the differential cross section is included in the systematic error of Table 5. However, because of difficulties in the

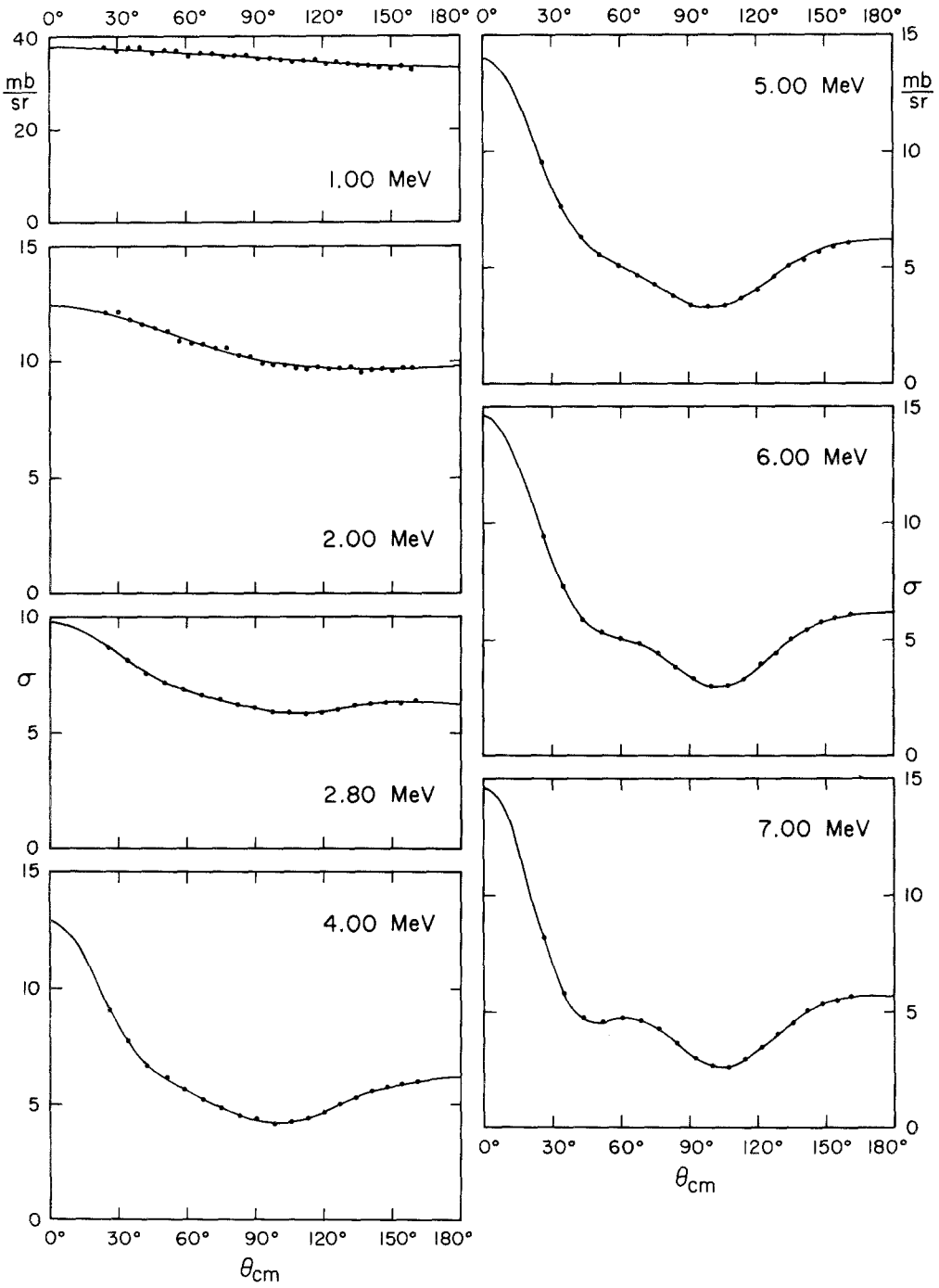

Fig. 2. Differential cross sections of the $^3He(d, p)^4He$ reaction between 1.0 and 7.0 MeV. The curves are Legendre-polynomial fits

measurement of the absolute beam intensity at $E_d = 1$ and 2 MeV these data were normalized by the results of Neng-Ming [20] at an angle of $\theta_{lab} = 90°$. These problems appear due to the loss of deuterons caused by the scattering in the windows of the gas target at these low energies. The uncertainty of the absolute value at 1

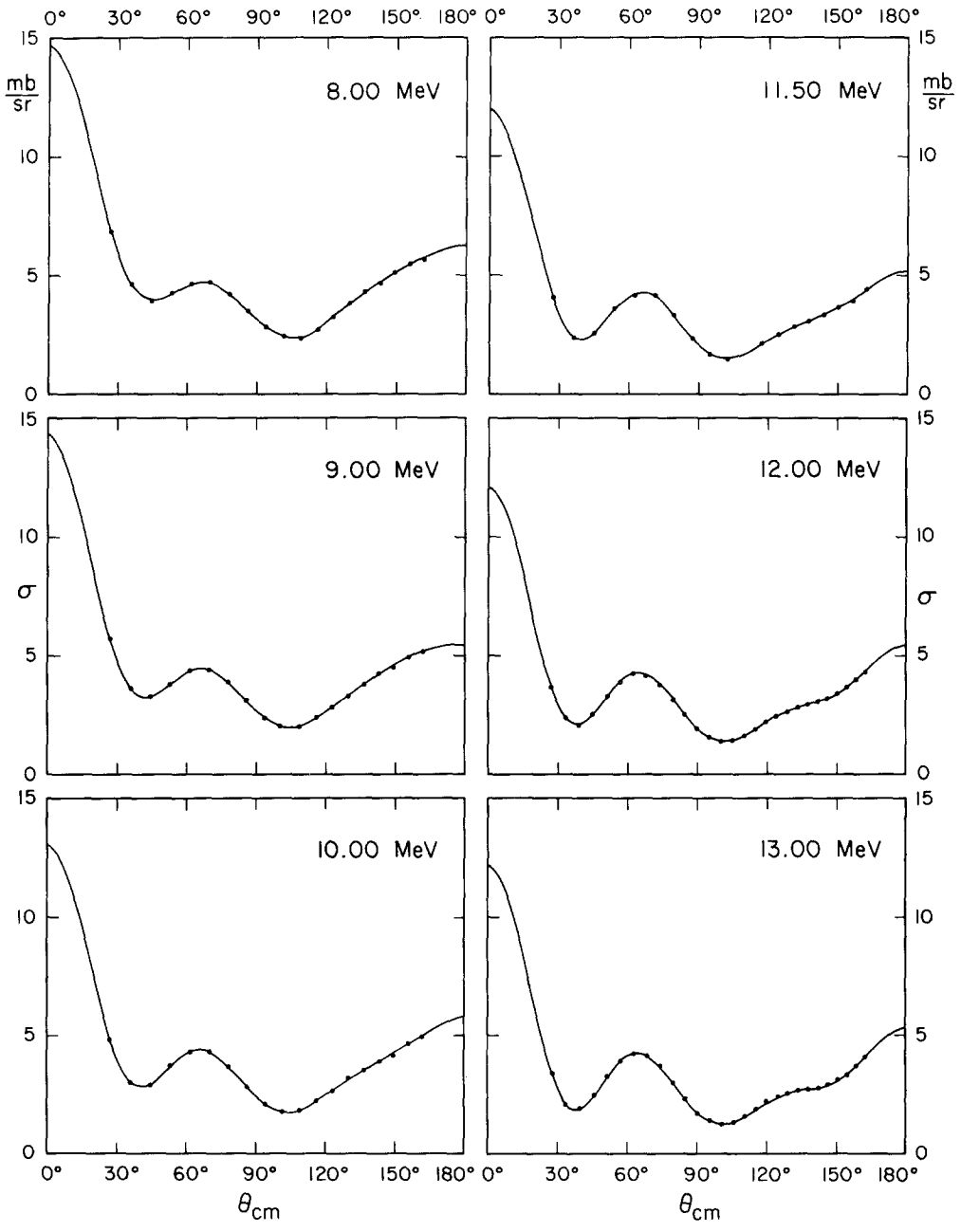

Fig. 3. Differential cross sections of the $^3He(d, p)^4He$ reaction between 8.0 and 13.0 MeV. The curves are Legendre-polynomial fits

and 2 MeV is therefore about 6%. Losses of protons due to interactions in the silicon detectors are negligibly small at the energies in this experiment. Proton contamination in the primary beam due to deuteron disintegration by the collimator is discriminated in the detectors by the high Q-value of the $^3He(d, p)^4He$ reaction.

Table 2. Differential cross section in mb/sr

1.0 MeV		2.0 MeV		12.0 MeV		13.0 MeV	
θ_{cm} (deg)	$d\sigma/d\Omega$	θ_{cm} (deg)	$d\sigma/d\Omega$	θ_{cm} (deg)	$d\sigma/d\Omega$	θ_{cm} (deg)	$d\sigma/d\Omega$
24.1	37.61	24.7	12.10	27.3	3.66	27.4	3.35
29.4	36.76	30.2	12.16	33.2	2.37	33.4	2.06
34.7	37.61	35.6	11.82	39.2	2.06	39.4	1.87
40.0	37.68	41.0	11.59	45.1	2.52	45.3	2.42
45.3	36.41	46.4	11.44	50.9	3.26	51.2	3.23
50.6	37.11	51.8	11.33	56.7	3.84	57.0	3.86
55.8	37.15	57.1	10.85	62.4	4.23	62.7	4.17
61.0	35.91	62.4	10.81	68.0	4.14	68.3	4.08
66.2	36.41	67.6	10.75	73.6	3.76	73.9	3.65
71.5	36.30	72.9	10.58	79.1	3.15	79.4	2.95
76.5	35.70	78.0	10.58	84.4	2.52	84.8	2.27
81.6	36.06	83.2	10.25	89.7	1.94	90.1	1.69
86.5	35.95	88.3	10.21	94.9	1.54	95.3	1.36
91.7	35.21	93.3	9.90	100.0	1.38	100.4	1.23
96.7	35.35	98.3	9.86	105.0	1.39	105.4	1.29
101.5	34.96	103.3	9.84	109.9	1.60	110.3	1.53
106.6	34.68	108.2	9.72	114.7	1.89	115.1	1.84
111.5	35.00	113.0	9.69	119.4	2.17	119.8	2.13
116.5	35.17	117.9	9.76	124.1	2.44	124.4	2.36
121.2	34.19	122.6	9.70	128.6	2.63	128.9	2.50
126.0	34.79	127.4	9.73	133.0	2.80	133.3	2.62
131.0	34.19	132.1	9.76	137.4	2.93	137.7	2.68
135.6	33.98	136.8	9.53	141.7	3.05	142.0	2.72
140.0	34.08	141.4	9.66	145.9	3.17	146.2	2.88
145.0	33.45	146.0	9.70	150.1	3.41	150.3	3.07
149.8	34.29	150.6	9.59	154.2	3.67	154.4	3.30
154.5	33.94	155.2	9.77	158.2	3.98	158.4	3.67
159.0	33.02	159.7	9.73	162.3	4.30	162.4	4.04

Table 3. Total cross section $\sigma_{tot}/4\pi = a_{00}(0)$ in mb

E_d (MeV)	$\sigma_{tot}/4\pi$
1.0	35.55 ± 0.07
2.0	10.42 ± 0.02
2.8	6.60 ± 0.01
4.0	5.48 ± 0.02
5.0	5.13 ± 0.02
6.0	4.98 ± 0.02
7.0	4.54 ± 0.02
8.0	4.19 ± 0.02
9.0	3.76 ± 0.02
10.0	3.46 ± 0.02
11.5	3.08 ± 0.02
12.0	3.00 ± 0.01
13.0	2.85 ± 0.01

Table 4. Normalized Legendre polynomial coefficients $d_{00}(L) = a_{00}(L)/a_{00}(0)$ from the analysis of the differential cross section

E_d (MeV)	$d_{00}(1)$	$d_{00}(2)$	$d_{00}(3)$	$d_{00}(4)$	$d_{00}(5)$
1.0	0.0579 (33)				
2.0	0.1261 (30)	0.0644 (40)			
2.8	0.1693 (30)	0.1861 (41)	0.0490 (53)	0.0365 (59)	0.0459 (67)
4.0	0.2663 (74)	0.5025 (120)	0.1607 (138)	0.1264 (174)	0.1530 (168)
5.0	0.3099 (84)	0.7051 (113)	0.1923 (152)	0.1757 (160)	0.2408 (183)
6.0	0.3325 (69)	0.7366 (101)	0.1620 (119)	0.2292 (140)	0.3524 (127)
7.0	0.3154 (79)	0.7095 (108)	0.1296 (141)	0.3299 (145)	0.5051 (167)
8.0	0.2739 (100)	0.6823 (162)	0.0486 (185)	0.4206 (219)	0.6109 (208)
9.0	0.2708 (128)	0.6691 (181)	0.0101 (250)	0.4674 (250)	0.7268 (279)
10.0	0.2485 (97)	0.6384 (156)	−0.0879 (175)	0.4536 (203)	0.7489 (196)
11.5	0.2728 (127)	0.6068 (205)	−0.1350 (221)	0.4250 (260)	0.8218 (250)
12.0	0.2742 (68)	0.5996 (109)	−0.1715 (120)	0.4174 (139)	0.8291 (132)
13.0	0.3082 (74)	0.5989 (118)	−0.1747 (128)	0.4182 (148)	0.8705 (142)

E_d (MeV)	$d_{00}(6)$	$d_{00}(7)$	$d_{00}(8)$	$d_{00}(9)$
4.0	0.0781 (188)	0.0391 (154)	0.0295 (155)	
5.0	0.0998 (154)	0.0189 (154)		
6.0	0.1255 (130)			
7.0	0.2102 (141)	0.0403 (141)		
8.0	0.3306 (232)	0.0765 (185)	0.0495 (182)	
9.0	0.4462 (247)	0.1321 (268)	0.0547 (199)	0.0303 (191)
10.0	0.5505 (222)	0.1257 (180)	0.0735 (177)	
11.5	0.7070 (280)	0.1408 (228)	0.0537 (244)	
12.0	0.8001 (151)	0.1678 (120)	0.0979 (116)	
13.0	0.9312 (162)	0.1933 (129)	0.1201 (124)	

Table 5. Systematic errors

Geometry factor $\Delta G/G$	1.2%
Beam position changes $\Delta\sigma/\sigma$	$\leqslant$ 0.013%
Density of the target gas	0.2%
Analysis of the spectra	0.5%
Charge determination (current integrator)	0.5%
Total systematic errors	1.3%

4.2 Analyzing Powers

Angular distributions were measured for the vector-analyzing power iT_{11} and the three tensor-analyzing powers T_{20}, T_{21} and T_{22}. This investigation was performed at 1 and 13 MeV and between 2 and 12 MeV in steps of 2 MeV. The angular range of these measurements extended from $\theta_{lab} = 10°$ to 170° in steps of 5°. The statistical errors of the results vary between 0.004 and 0.009. The results are presented

in Figs. 4 to 7. The data points in these figures are larger than the statistical errors. The curves are Legendre-polynomial fits. Numerical values of the data are given in Tables 6a to 6h. The normalized Legendre-polynomial coefficients $d_{kq}(L) = a_{kq}(L)/a_{00}(0)$ are presented in Tables 7a to 7d.

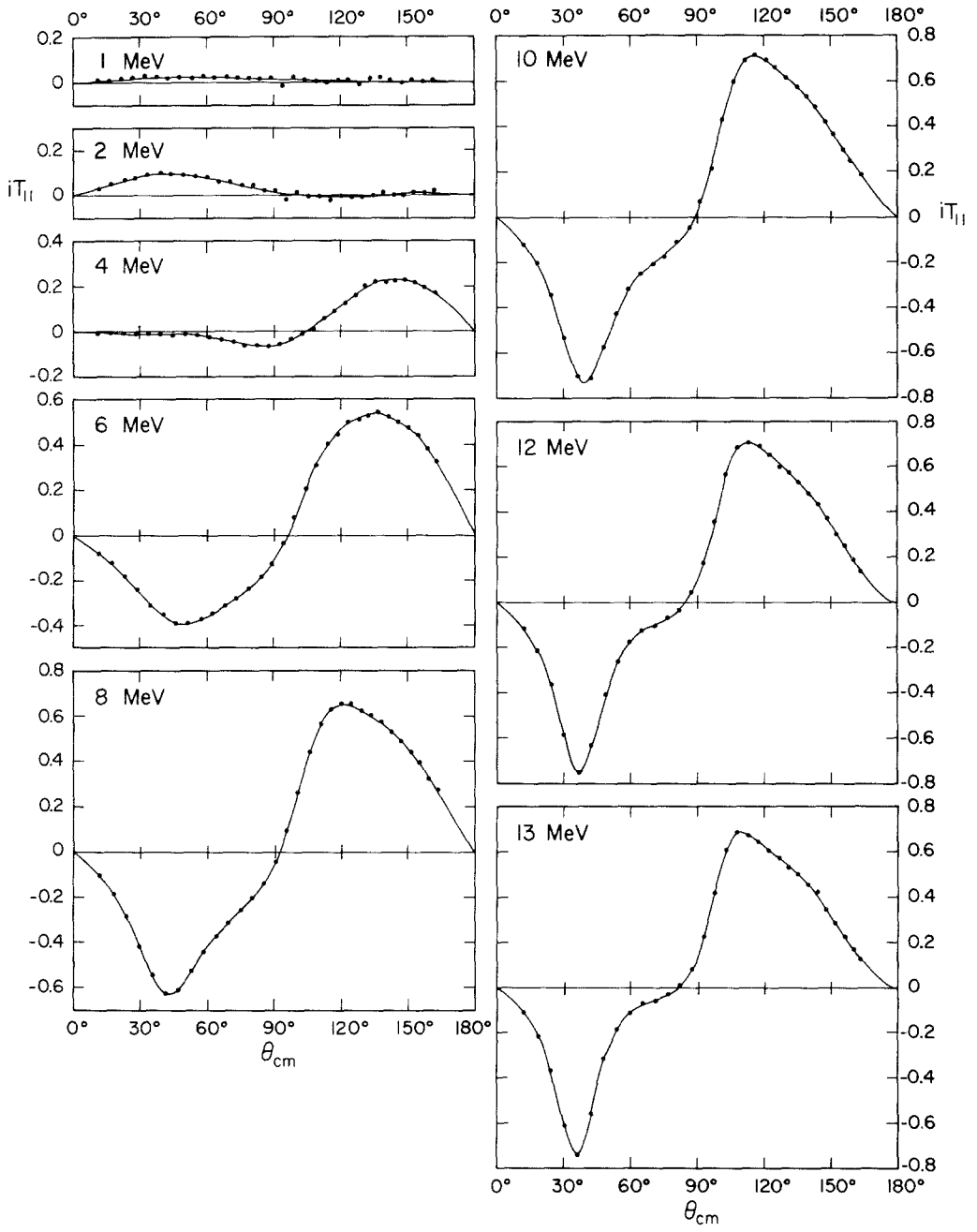

Fig. 4. Vector-analyzing powers iT_{11} as a function of scattering angle between 1.0 and 13.0 MeV. The curves are Legendre-polynomial fits

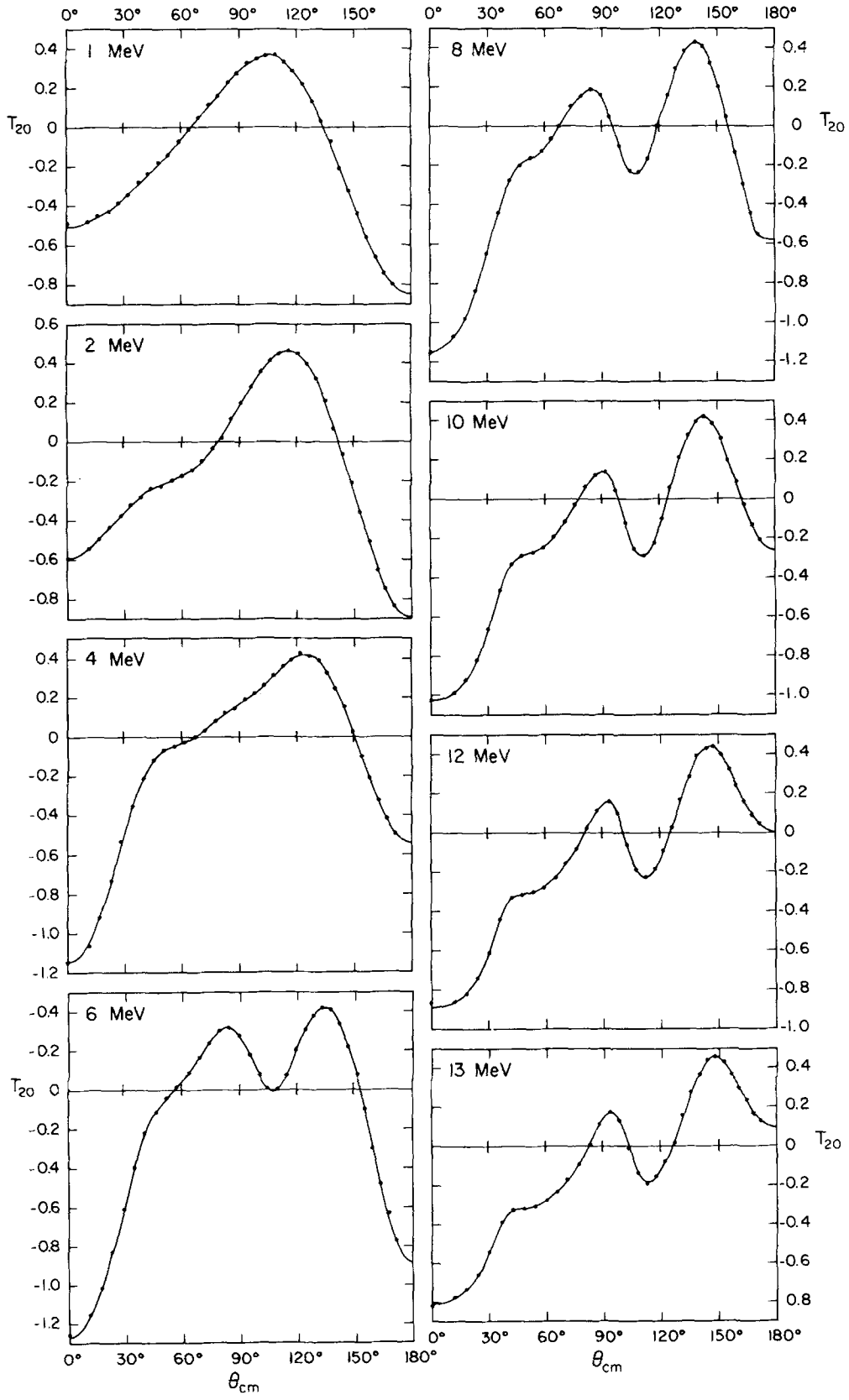

Fig. 5. Tensor-analyzing powers T_{20} as a function of scattering angle between 1.0 and 13.0 MeV. The curves are Legendre-polynomial fits

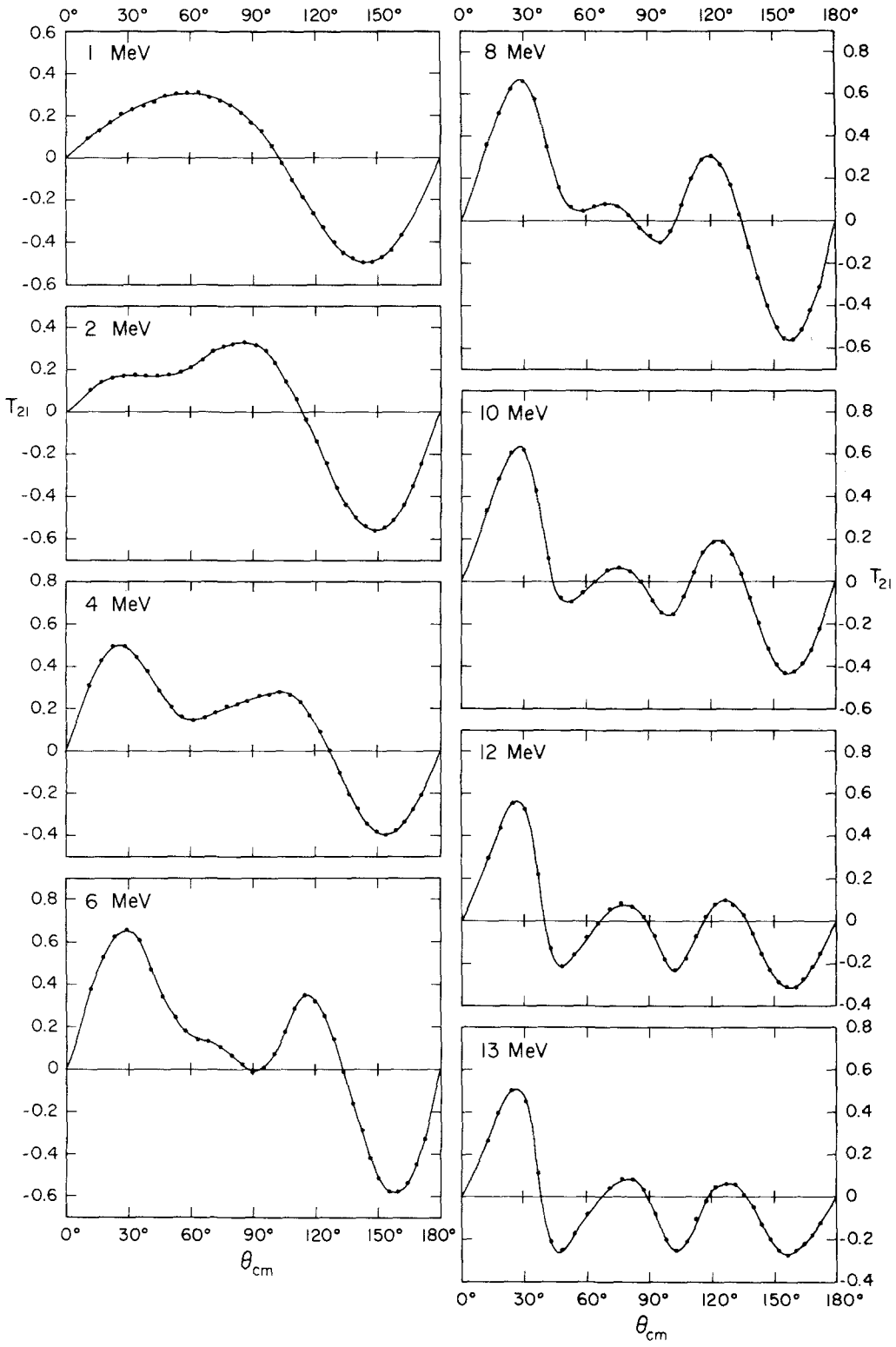

Fig. 6. Tensor-analyzing powers T_{21} as a function of scattering angle between 1.0 and 13.0 MeV. The curves are Legendre-polynomial fits

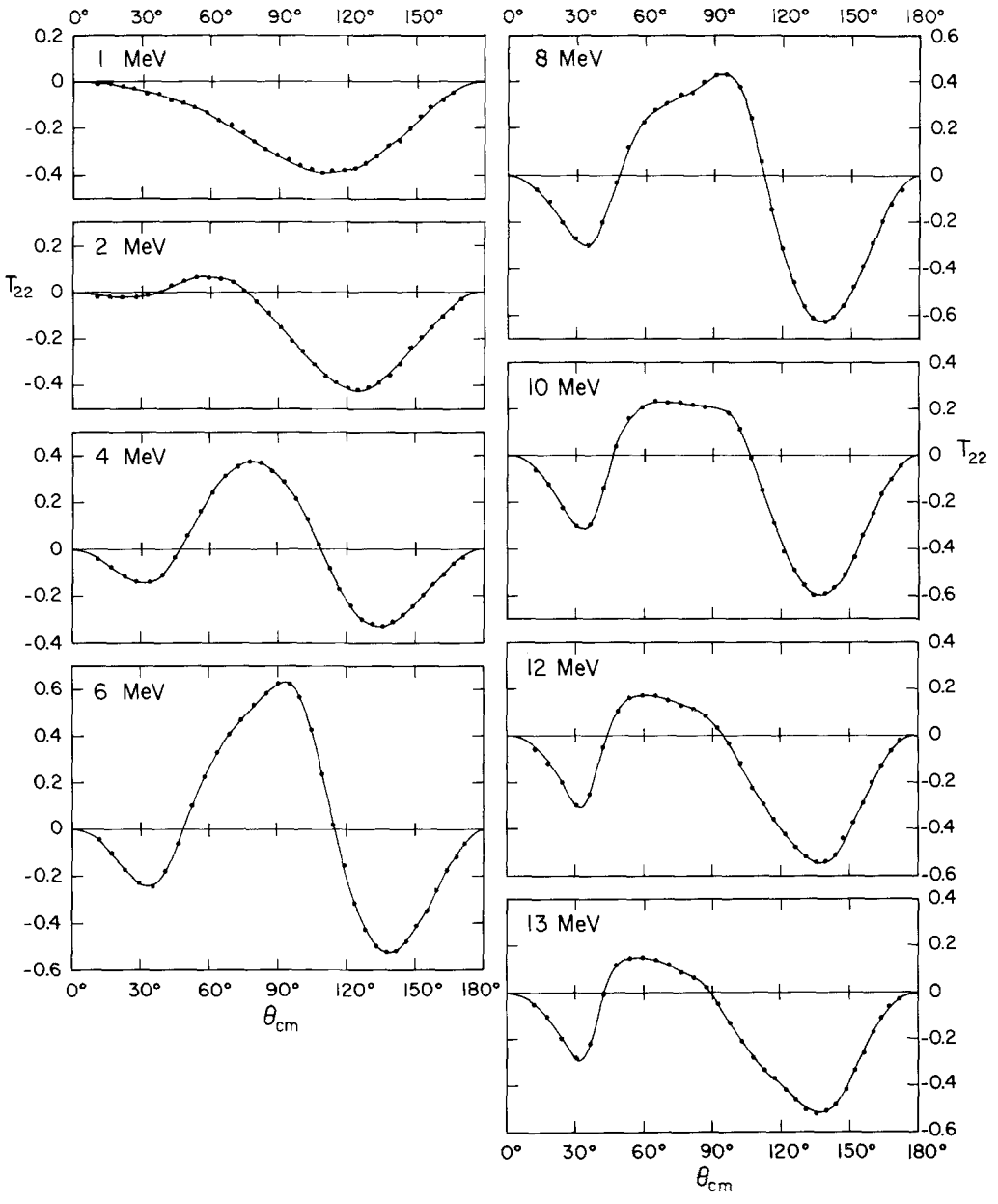

Fig. 7. Tensor-analyzing powers T_{22} as a function of scattering angle between 1.0 and 13.0 MeV. The curves are Legendre-polynomial fits

4.2.1 Finite-Size Corrections

The finite size of the solid angle given by the slit system and the diaphragms may require a correction in the analyzing-power results. This problem is particularly critical for the extreme forward and backward angles. For the determination of the quantities T_{kq} from the detector counting rates, values of the beam polarization t_{kq} are used which correspond to a point geometry of the detectors. In reality, however, the diaphragms in front of the detectors have an extension $\pm \Delta\phi$ in direction of the aximuthal angle ϕ. A deviation $\Delta\phi$ corresponds to a rotation of the normal of the

Table 6 a. Analyzing powers of the reaction $^3He(\vec{d}, p)^4He$ at 1 MeV

θ_{lab}	θ_{cm}	iT_{11}	ΔiT_{11}	T_{20}	ΔT_{20}	T_{21}	ΔT_{21}	T_{22}	ΔT_{22}
10.0	10.7	0.0120	0.0042	−0.4791	0.0078	0.0929	0.0046	−0.0085	0.0040
15.0	16.1	0.0128	0.0031	−0.4533	0.0070	0.1314	0.0038	−0.0120	0.0031
20.0	21.4	0.0188	0.0028	−0.4276	0.0065	0.1698	0.0038	−0.0221	0.0027
25.0	26.8	0.0225	0.0028	−0.3859	0.0060	0.2086	0.0041	−0.0327	0.0028
30.0	32.1	0.0314	0.0049	−0.3439	0.0079	0.2312	0.0071	−0.0519	0.0057
35.0	37.4	0.0242	0.0037	−0.2829	0.0063	0.2515	0.0059	−0.0545	0.0045
40.0	42.7	0.0230	0.0032	−0.2433	0.0054	0.2666	0.0055	−0.0803	0.0039
45.0	48.0	0.0237	0.0031	−0.1819	0.0048	0.2940	0.0056	−0.0928	0.0038
50.0	53.2	0.0233	0.0047	−0.1378	0.0049	0.3052	0.0066	−0.1075	0.0046
55.0	58.4	0.0286	0.0043	−0.0692	0.0048	0.3081	0.0068	−0.1349	0.0049
60.0	63.6	0.0181	0.0033	−0.0115	0.0048	0.3138	0.0070	−0.1667	0.0032
65.0	68.8	0.0234	0.0033	0.0487	0.0050	0.2906	0.0070	−0.1857	0.0054
70.0	73.9	0.0233	0.0043	0.1144	0.0059	0.2764	0.0073	−0.2220	0.0058
75.0	79.0	0.0220	0.0033	0.1582	0.0062	0.2495	0.0072	−0.2626	0.0062
80.0	84.1	0.0161	0.0030	0.2270	0.0066	0.2146	0.0071	−0.2902	0.0064
85.0	89.2	0.0169	0.0091	0.2761	0.0070	0.1715	0.0071	−0.3163	0.0066
90.0	94.2	−0.0144	0.0107	0.3279	0.0069	0.1272	0.0053	−0.3343	0.0066
95.0	99.2	0.0236	0.0107	0.3468	0.0071	0.0525	0.0050	−0.3603	0.0068
100.0	104.1	0.0098	0.0106	0.3662	0.0072	−0.0246	0.0050	−0.3747	0.0069
105.0	109.0	0.0051	0.0086	0.3718	0.0050	−0.1055	0.0080	−0.3899	0.0052
110.0	113.9	0.0014	0.0085	0.3352	0.0055	−0.1843	0.0064	−0.3824	0.0075
115.0	118.8	0.0107	0.0085	0.2904	0.0054	−0.2679	0.0046	−0.3791	0.0074
120.0	123.6	0.0074	0.0075	0.2209	0.0036	−0.3280	0.0044	−0.3715	0.0050
125.0	128.4	−0.0070	0.0083	0.1292	0.0056	−0.3998	0.0058	−0.3489	0.0072
130.0	133.2	0.0159	0.0081	0.0278	0.0053	−0.4506	0.0040	−0.3182	0.0070
135.0	137.9	0.0215	0.0078	−0.0668	0.0048	−0.4737	0.0050	−0.2746	0.0051
140.0	142.7	0.0070	0.0070	−0.2094	0.0053	−0.4958	0.0049	−0.2547	0.0066
145.0	147.4	0.0037	0.0071	−0.3273	0.0055	−0.4923	0.0050	−0.2024	0.0061
150.0	152.1	0.0119	0.0067	−0.4422	0.0057	−0.4670	0.0064	−0.1513	0.0041
155.0	156.8	0.0034	0.0060	−0.5578	0.0043	−0.4347	0.0060	−0.1121	0.0053
160.0	161.4	0.0089	0.0055	−0.6597	0.0066	−0.3641	0.0054	−0.0801	0.0047
165.0	166.1			−0.7442	0.0075			−0.0430	0.0042
169.7	170.4			−0.8010	0.0075				

Table 6 b. Analyzing powers of the reaction $^3He(\vec{d}, p)^4He$ at 2 MeV

θ_{lab}	θ_{cm}	iT_{11}	ΔiT_{11}	T_{20}	ΔT_{20}	T_{21}	ΔT_{21}	T_{22}	ΔT_{22}
10.0	11.0	0.0292	0.0043	−0.5481	0.0085	0.0985	0.0036	−0.0171	0.0039
15.0	16.5	0.0479	0.0033	−0.5000	0.0074	0.1389	0.0028	−0.0169	0.0030
20.0	22.0	0.0673	0.0030	−0.4376	0.0066	0.1578	0.0026	−0.0217	0.0027
25.0	27.5	0.0762	0.0031	−0.3819	0.0060	0.1712	0.0027	−0.0205	0.0028
30.0	32.9	0.0934	0.0053	−0.3238	0.0070	0.1726	0.0044	−0.0078	0.0058
35.0	38.3	0.0984	0.0042	−0.2838	0.0057	0.1691	0.0034	0.0032	0.0044
40.0	43.7	0.0949	0.0036	−0.2418	0.0049	0.1709	0.0030	0.0330	0.0039
45.0	49.1	0.0911	0.0035	−0.2267	0.0047	0.1759	0.0030	0.0485	0.0038
50.0	54.5	0.0842	0.0061	−0.1976	0.0048	0.1933	0.0032	0.0654	0.0045
55.0	59.8	0.0798	0.0051	−0.1810	0.0049	0.2128	0.0034	0.0646	0.0047
60.0	65.0	0.0621	0.0054	−0.1443	0.0048	0.2447	0.0036	0.0629	0.0049
65.0	70.3	0.0592	0.0039	−0.1010	0.0048	0.2882	0.0051	0.0435	0.0050
70.0	75.5	0.0458	0.0063	−0.0314	0.0057	0.3089	0.0060	0.0065	0.0053
75.0	80.6	0.0440	0.0061	0.0224	0.0059	0.3206	0.0062	−0.0390	0.0054
80.0	85.7	0.0218	0.0049	0.1139	0.0062	0.3328	0.0064	−0.0911	0.0055
85.0	90.8	0.0169	0.0087	0.1990	0.0067	0.3152	0.0063	−0.1482	0.0057
90.0	95.8	−0.0176	0.0087	0.2820	0.0063	0.2901	0.0054	−0.2130	0.0055
95.0	100.8	0.0079	0.0088	0.3637	0.0070	0.2333	0.0050	−0.2561	0.0056
100.0	105.7	−0.0066	0.0088	0.4157	0.0075	0.1447	0.0044	−0.3077	0.0056
105.0	110.6	−0.0063	0.0063	0.4533	0.0058	0.0586	0.0056	−0.3638	0.0045
110.0	115.5	−0.0234	0.0091	0.4640	0.0086	−0.0337	0.0059	−0.3918	0.0077
115.0	120.3	−0.0059	0.0093	0.4506	0.0085	−0.1419	0.0059	−0.4138	0.0078
120.0	125.0	−0.0131	0.0079	0.3972	0.0074	−0.2406	0.0053	−0.4219	0.0072
125.0	129.8	−0.0082	0.0086	0.3171	0.0075	−0.3597	0.0069	−0.4116	0.0073
130.0	134.5	−0.0064	0.0082	0.2080	0.0068	−0.4378	0.0068	−0.3881	0.0071
135.0	139.1	0.0095	0.0080	0.0660	0.0063	−0.5012	0.0069	−0.3598	0.0068
140.0	143.7	0.0001	0.0073	−0.0653	0.0109	−0.5433	0.0045	−0.3087	0.0056
145.0	148.3	−0.0024	0.0074	−0.2125	0.0061	−0.5572	0.0060	−0.2424	0.0064
150.0	152.9	0.0131	0.0069	−0.3538	0.0066	−0.5524	0.0058	−0.1955	0.0058
155.0	157.5	0.0126	0.0065	−0.5111	0.0081	−0.5085	0.0038	−0.1541	0.0039
160.0	162.0	0.0246	0.0059	−0.6553	0.0089	−0.4432	0.0050	−0.1044	0.0048
165.0	166.5			−0.7523	0.0095	−0.3514	0.0044	−0.0695	0.0042
169.7	170.7			−0.8371	0.0104	−0.2465	0.0044	−0.0324	0.0045

Table 6c. Analyzing powers of the reaction $^3He(\vec{d}, p)^4He$ at 4 MeV

θ_{lab}	θ_{cm}	iT_{11}	ΔiT_{11}	T_{20}	ΔT_{20}	T_{21}	ΔT_{21}	T_{22}	ΔT_{22}
10.0	11.4	−0.0073	0.0044	−1.0663	0.0024	0.3193	0.0033	−0.0368	0.0023
15.0	17.1	−0.0058	0.0033	−0.9179	0.0021	0.4314	0.0027	−0.0752	0.0019
20.0	22.7	−0.0104	0.0030	−0.7335	0.0026	0.5003	0.0026	−0.1138	0.0018
25.0	28.4	−0.0156	0.0023	−0.5364	0.0014	0.5000	0.0025	−0.1380	0.0039
30.0	34.0	−0.0118	0.0036	−0.3548	0.0029	0.4458	0.0044	−0.1423	0.0044
35.0	39.6	−0.0164	0.0032	−0.2139	0.0036	0.3775	0.0041	−0.1080	0.0040
40.0	45.1	−0.0185	0.0038	−0.1216	0.0024	0.2917	0.0027	−0.0338	0.0032
45.0	50.7	−0.0166	0.0050	−0.0714	0.0029	0.2100	0.0045	0.0625	0.0040
50.0	56.1	−0.0203	0.0054	−0.0473	0.0031	0.1648	0.0041	0.1628	0.0043
55.0	61.5	−0.0300	0.0058	−0.0292	0.0034	0.1532	0.0045	0.2459	0.0046
60.0	66.9	−0.0393	0.0045	0.0019	0.0057	0.1595	0.0047	0.3131	0.0045
65.0	72.3	−0.0509	0.0047	0.0314	0.0060	0.1851	0.0050	0.3545	0.0048
70.0	77.5	−0.0653	0.0049	0.0789	0.0062	0.2137	0.0051	0.3735	0.0050
75.0	82.7	−0.0669	0.0034	0.1205	0.0066	0.2243	0.0077	0.3685	0.0053
80.0	87.9	−0.0671	0.0048	0.1405	0.0041	0.2387	0.0047	0.3337	0.0053
85.0	93.0	−0.0611	0.0049	0.1923	0.0042	0.2650	0.0048	0.2868	0.0055
90.0	98.0	−0.0437	0.0039	0.2190	0.0031	0.2722	0.0028	0.2128	0.0056
95.0	103.0	−0.0136	0.0062	0.2589	0.0030	0.2770	0.0034	0.1284	0.0033
100.0	107.9	0.0091	0.0062	0.3076	0.0042	0.2723	0.0048	0.0233	0.0041
105.0	112.7	0.0562	0.0062	0.3629	0.0042	0.2346	0.0047	−0.0826	0.0040
110.0	117.5	0.0845	0.0069	0.3902	0.0050	0.1734	0.0053	−0.1700	0.0049
115.0	122.3	0.1203	0.0066	0.4240	0.0049	0.0898	0.0051	−0.2423	0.0048
120.0	126.9	0.1559	0.0066	0.4105	0.0048	0.0004	0.0049	−0.2989	0.0047
125.0	131.6	0.2001	0.0064	0.3908	0.0046	−0.1019	0.0047	−0.3202	0.0046
130.0	136.1	0.2139	0.0065	0.3207	0.0050	−0.1968	0.0040	−0.3288	0.0045
135.0	140.6	0.2149	0.0062	0.2472	0.0047	−0.2710	0.0039	−0.3127	0.0043
140.0	145.1	0.2217	0.0059	0.1500	0.0044	−0.3422	0.0039	−0.2828	0.0041
145.0	149.6	0.2253	0.0041	0.0232	0.0031	−0.3735	0.0034	−0.2429	0.0062
150.0	154.0	0.2081	0.0055	−0.1050	0.0030	−0.3900	0.0034	−0.1948	0.0035
155.0	158.4	0.1892	0.0051	−0.2150	0.0034	−0.3670	0.0028	−0.1493	0.0029
160.0	162.7	0.1642	0.0046	−0.3301	0.0028	−0.3369	0.0025	−0.1073	0.0025
165.0	167.1			−0.4213	0.0031	−0.2697	0.0050	−0.0613	0.0029
169.7	171.1			−0.5002	0.0063	−0.1873	0.0050	−0.0454	0.0051

Table 6d. Analyzing powers of the reaction $^3He(\vec{d}, p)^4He$ at 6 MeV

θ_{lab}	θ_{cm}	iT_{11}	ΔiT_{11}	T_{20}	ΔT_{20}	T_{21}	ΔT_{21}	T_{22}	ΔT_{22}
10.0	11.6	−0.0783	0.0026	−1.1546	0.0045	0.3807	0.0026	−0.0439	0.0035
15.0	17.5	−0.1218	0.0027	−1.0148	0.0040	0.5279	0.0025	−0.1024	0.0030
20.0	23.3	−0.1802	0.0035	−0.8284	0.0035	0.6281	0.0027	−0.1748	0.0029
25.0	29.0	−0.2392	0.0038	−0.6084	0.0043	0.6574	0.0025	−0.2267	0.0055
30.0	34.8	−0.3091	0.0074	−0.3949	0.0049	0.6068	0.0044	−0.2449	0.0054
35.0	40.5	−0.3513	0.0077	−0.2212	0.0040	0.4732	0.0041	−0.1807	0.0047
40.0	46.1	−0.3866	0.0053	−0.1126	0.0044	0.3436	0.0039	−0.0610	0.0054
45.0	51.7	−0.3867	0.0063	−0.0387	0.0039	0.2445	0.0045	0.0980	0.0040
50.0	57.3	−0.3729	0.0064	0.0138	0.0041	0.1798	0.0047	0.2259	0.0043
55.0	62.8	−0.3445	0.0067	0.0869	0.0044	0.1420	0.0050	0.3298	0.0045
60.0	68.3	−0.3066	0.0058	0.1638	0.0046	0.1322	0.0043	0.4099	0.0048
65.0	73.6	−0.2776	0.0061	0.2372	0.0050	0.1046	0.0046	0.4744	0.0052
70.0	79.0	−0.2359	0.0064	0.3060	0.0053	0.0656	0.0049	0.5369	0.0055
75.0	84.2	−0.1846	0.0045	0.3179	0.0057	0.0249	0.0053	0.5848	0.0059
80.0	89.4	−0.1287	0.0065	0.2803	0.0056	−0.0193	0.0044	0.6256	0.0053
85.0	94.5	−0.0351	0.0067	0.1804	0.0059	0.0066	0.0047	0.6249	0.0055
90.0	99.6	0.0814	0.0043	0.0780	0.0039	0.0728	0.0033	0.5692	0.0041
95.0	104.5	0.2045	0.0056	0.0076	0.0075	0.1748	0.0046	0.4311	0.0055
100.0	109.4	0.3128	0.0059	0.0081	0.0050	0.2851	0.0048	0.2382	0.0052
105.0	114.2	0.4054	0.0060	0.0759	0.0049	0.3484	0.0048	0.0234	0.0049
110.0	119.0	0.4457	0.0062	0.2049	0.0053	0.3241	0.0052	−0.1549	0.0054
115.0	123.6	0.4986	0.0062	0.3059	0.0052	0.2508	0.0048	−0.3162	0.0053
120.0	128.3	0.5094	0.0060	0.3779	0.0051	0.1365	0.0045	−0.4319	0.0052
125.0	132.8	0.5314	0.0059	0.4198	0.0050	−0.0115	0.0042	−0.4996	0.0051
130.0	137.3	0.5397	0.0074	0.4114	0.0049	−0.1568	0.0035	−0.5244	0.0047
135.0	141.7	0.5245	0.0070	0.3429	0.0044	−0.2925	0.0036	−0.5210	0.0045
140.0	146.1	0.5025	0.0066	0.2213	0.0040	−0.4226	0.0038	−0.4816	0.0044
145.0	150.5	0.4755	0.0043	0.0806	0.0054	−0.5155	0.0097	−0.4149	0.0031
150.0	154.8	0.4434	0.0057	−0.1005	0.0046	−0.5788	0.0048	−0.3512	0.0046
155.0	159.0	0.3850	0.0051	−0.3003	0.0048	−0.5792	0.0034	−0.2590	0.0035
160.0	163.3	0.3264	0.0045	−0.4840	0.0035	−0.5378	0.0034	−0.1771	0.0036
165.0	167.5			−0.6316	0.0039	−0.4468	0.0050	−0.1159	0.0043
169.7	171.4			−0.7777	0.0066	−0.3269	0.0049	−0.0627	0.0044

Table 6e. Analyzing powers of the reaction $^3He(\vec{d}, p)^4He$ at 8 MeV

θ_{lab}	θ_{cm}	iT_{11}	ΔiT_{11}	T_{20}	ΔT_{20}	T_{21}	ΔT_{21}	T_{22}	ΔT_{22}
10.0	11.9	−0.1032	0.0042	−1.0730	0.0035	0.3561	0.0030	−0.0574	0.0037
15.0	17.8	−0.1850	0.0044	−0.9802	0.0029	0.5121	0.0029	−0.1109	0.0032
20.0	23.7	−0.2828	0.0058	−0.8391	0.0028	0.6267	0.0031	−0.1993	0.0034
25.0	29.5	−0.4155	0.0063	−0.6468	0.0042	0.6659	0.0078	−0.2719	0.0078
30.0	35.3	−0.5382	0.0113	−0.4423	0.0053	0.5806	0.0043	−0.2997	0.0048
35.0	41.1	−0.6247	0.0122	−0.2749	0.0050	0.3534	0.0041	−0.1997	0.0046
40.0	46.9	−0.6066	0.0050	−0.1984	0.0028	0.1606	0.0031	−0.0287	0.0067
45.0	52.6	−0.5251	0.0053	−0.1642	0.0036	0.0656	0.0051	0.1198	0.0049
50.0	58.2	−0.4375	0.0049	−0.1287	0.0036	0.0469	0.0050	0.2307	0.0049
55.0	63.8	−0.3721	0.0050	−0.0609	0.0065	0.0669	0.0053	0.2772	0.0051
60.0	69.3	−0.3115	0.0042	−0.0009	0.0038	0.0758	0.0053	0.3082	0.0041
65.0	74.7	−0.2547	0.0043	0.0972	0.0041	0.0696	0.0047	0.3434	0.0045
70.0	80.1	−0.2033	0.0044	0.1553	0.0044	0.0272	0.0050	0.3540	0.0048
75.0	85.4	−0.1361	0.0031	0.1865	0.0048	−0.0346	0.0056	0.3978	0.0053
80.0	90.6	−0.0404	0.0044	0.1604	0.0050	−0.0687	0.0048	0.4270	0.0053
85.0	95.7	0.0988	0.0048	0.0474	0.0055	−0.1034	0.0052	0.4315	0.0057
90.0	100.8	0.2701	0.0040	−0.1032	0.0037	−0.0494	0.0087	0.3781	0.0039
95.0	105.7	0.4452	0.0067	−0.2249	0.0046	0.0723	0.0046	0.2459	0.0040
100.0	110.6	0.5657	0.0071	−0.2328	0.0049	0.1967	0.0048	0.0571	0.0051
105.0	115.4	0.6338	0.0071	−0.1582	0.0048	0.2906	0.0046	−0.1445	0.0049
110.0	120.1	0.6574	0.0077	−0.0052	0.0053	0.3053	0.0044	−0.3139	0.0050
115.0	124.7	0.6577	0.0075	0.1557	0.0049	0.2646	0.0041	−0.4540	0.0048
120.0	129.3	0.6307	0.0070	0.2944	0.0048	0.1673	0.0039	−0.5574	0.0046
125.0	133.8	0.6113	0.0066	0.3887	0.0046	0.0293	0.0036	−0.6129	0.0045
130.0	138.2	0.5789	0.0072	0.4262	0.0045	−0.1248	0.0044	−0.6263	0.0046
135.0	142.6	0.5297	0.0067	0.4088	0.0042	−0.2692	0.0042	−0.6035	0.0044
140.0	146.9	0.4953	0.0063	0.3204	0.0039	−0.4027	0.0041	−0.5549	0.0041
145.0	151.1	0.4445	0.0041	0.2031	0.0022	−0.5009	0.0031	−0.4759	0.0031
150.0	155.4	0.3981	0.0053	0.0454	0.0051	−0.5538	0.0045	−0.3870	0.0048
155.0	159.5	0.3290	0.0047	−0.1334	0.0033	−0.5566	0.0031	−0.2881	0.0056
160.0	163.7	0.2776	0.0042	−0.2972	0.0055	−0.5159	0.0088	−0.2004	0.0045
165.0	167.8			−0.4452	0.0048	−0.4213	0.0035	−0.1247	0.0030
169.7	171.6			−0.5564	0.0058	−0.3108	0.0033	−0.0678	0.0035

Table 6 f. Analyzing powers of the reaction $^3He(\vec{d}, p)^4He$ at 10 MeV

θ_{lab}	θ_{cm}	iT_{11}	ΔiT_{11}	T_{20}	ΔT_{20}	T_{21}	ΔT_{21}	T_{22}	ΔT_{22}
10.0	12.0	−0.1160	0.0041	−0.9895	0.0066	0.3337	0.0039	−0.0585	0.0032
15.0	18.0	−0.1977	0.0034	−0.9184	0.0051	0.4855	0.0043	−0.1195	0.0029
20.0	24.0	−0.3395	0.0047	−0.8207	0.0062	0.6081	0.0037	−0.2179	0.0047
25.0	29.9	−0.5269	0.0052	−0.6557	0.0042	0.6242	0.0038	−0.2990	0.0043
30.0	35.8	−0.7023	0.0076	−0.4598	0.0048	0.4287	0.0042	−0.2938	0.0039
35.0	41.7	−0.7064	0.0092	−0.3263	0.0042	0.1062	0.0030	−0.1363	0.0034
40.0	47.5	−0.5715	0.0052	−0.2847	0.0053	−0.0761	0.0044	0.0423	0.0049
45.0	53.3	−0.4242	0.0064	−0.2704	0.0053	−0.0962	0.0043	0.1621	0.0048
50.0	59.0	−0.3161	0.0042	−0.2437	0.0051	−0.0464	0.0042	0.2067	0.0046
55.0	64.6	−0.2446	0.0107	−0.1893	0.0057	0.0036	0.0045	0.2372	0.0051
60.0	70.1	−0.2036	0.0060	−0.1104	0.0040	0.0502	0.0033	0.2287	0.0036
65.0	75.6	−0.1704	0.0064	−0.0242	0.0044	0.0675	0.0036	0.2281	0.0039
70.0	81.0	−0.1044	0.0075	0.0645	0.0048	0.0483	0.0039	0.2208	0.0039
75.0	86.3	−0.0438	0.0042	0.1236	0.0056	0.0003	0.0045	0.2132	0.0051
80.0	91.6	0.0682	0.0056	0.1423	0.0070	−0.0891	0.0057	0.2455	0.0057
85.0	96.7	0.2181	0.0063	0.0459	0.0062	−0.1462	0.0051	0.1835	0.0051
90.0	101.7	0.4363	0.0047	−0.1186	0.0041	−0.1520	0.0036	0.1140	0.0073
95.0	106.7	0.6013	0.0069	−0.2480	0.0015	−0.0718	0.0050	−0.0101	0.0043
100.0	111.6	0.6937	0.0072	−0.2850	0.0050	0.0425	0.0049	−0.1474	0.0053
105.0	116.3	0.7117	0.0070	−0.2240	0.0047	0.1427	0.0044	−0.2926	0.0050
110.0	121.0	0.6940	0.0067	−0.0939	0.0054	0.1921	0.0045	−0.4069	0.0054
115.0	125.6	0.6649	0.0064	0.0621	0.0051	0.1883	0.0042	−0.4930	0.0052
120.0	130.1	0.6216	0.0059	0.2138	0.0050	0.1290	0.0039	−0.5552	0.0052
125.0	134.6	0.5818	0.0056	0.3270	0.0049	0.0426	0.0037	−0.5951	0.0052
130.0	139.0	0.5341	0.0055	0.3960	0.0048	−0.0757	0.0044	−0.5905	0.0054
135.0	143.3	0.4866	0.0051	0.4254	0.0048	−0.1955	0.0042	−0.5664	0.0048
140.0	147.5	0.4241	0.0046	0.3903	0.0045	−0.3160	0.0042	−0.5116	0.0049
145.0	151.7	0.3715	0.0050	0.3086	0.0031	−0.3893	0.0029	−0.4306	0.0078
150.0	155.8	0.3034	0.0045	0.2010	0.0042	−0.4292	0.0040	−0.3406	0.0052
155.0	159.9	0.2514	0.0040	0.0877	0.0037	−0.4263	0.0028	−0.2439	0.0033
160.0	164.0	0.1992	0.0035	−0.0261	0.0027	−0.3879	0.0025	−0.1666	0.0057
165.0	168.0			−0.1287	0.0041	−0.3214	0.0033	−0.1014	0.0036
169.7	171.7			−0.2043	0.0044	−0.2266	0.0035	−0.0438	0.0038

Table 6 g. Analyzing powers of the reaction $^3He(\vec{d}, p)^4He$ at 12 MeV

θ_{lab}	θ_{cm}	iT_{11}	ΔiT_{11}	T_{20}	ΔT_{20}	T_{21}	ΔT_{21}	T_{22}	ΔT_{22}
10.0	12.2	−0.1114	0.0038	−0.8653	0.0089	0.2979	0.0043	−0.0613	0.0034
15.0	18.2	−0.2112	0.0046	−0.8204	0.0055	0.4419	0.0047	−0.1207	0.0032
20.0	24.3	−0.3594	0.0068	−0.7404	0.0053	0.5568	0.0056	−0.2026	0.0038
25.0	30.3	−0.5812	0.0083	−0.6092	0.0040	0.5306	0.0070	−0.2999	0.0038
30.0	36.2	−0.7529	0.0151	−0.4377	0.0051	0.2190	0.0043	−0.2500	0.0050
35.0	42.2	−0.6286	0.0125	−0.3356	0.0074	−0.1332	0.0036	−0.0525	0.0038
40.0	48.0	−0.4025	0.0048	−0.3147	0.0033	−0.2151	0.0027	0.1034	0.0025
45.0	53.8	−0.2582	0.0051	−0.3020	0.0026	−0.1610	0.0019	0.1622	0.0021
50.0	59.6	−0.1719	0.0047	−0.2765	0.0037	−0.0791	0.0053	0.1725	0.0021
55.0	65.3	−0.1222	0.0049	−0.2275	0.0029	−0.0072	0.0021	0.1664	0.0024
60.0	70.8	−0.1037	0.0055	−0.1629	0.0041	0.0539	0.0035	0.1516	0.0038
65.0	76.4	−0.0658	0.0060	−0.0767	0.0047	0.0856	0.0038	0.1293	0.0042
70.0	81.8	−0.0324	0.0068	0.0272	0.0053	0.0677	0.0043	0.1119	0.0048
75.0	87.1	0.0520	0.0041	0.1150	0.0036	0.0214	0.0029	0.0852	0.0033
80.0	92.4	0.1799	0.0058	0.1586	0.0046	−0.0727	0.0038	0.0343	0.0042
85.0	97.5	0.3663	0.0068	0.0971	0.0050	−0.1838	0.0041	−0.0351	0.0045
90.0	102.6	0.5742	0.0025	−0.0599	0.0069	−0.2287	0.0034	−0.1236	0.0037
95.0	107.5	0.6899	0.0072	−0.1917	0.0061	−0.1742	0.0056	−0.2265	0.0063
100.0	112.4	0.7162	0.0072	−0.2260	0.0057	−0.0713	0.0053	−0.2968	0.0059
105.0	117.1	0.7017	0.0067	−0.1866	0.0054	0.0212	0.0050	−0.3589	0.0056
110.0	121.8	0.6609	0.0078	−0.0924	0.0058	0.0817	0.0047	−0.4252	0.0052
115.0	126.4	0.6002	0.0072	0.0263	0.0055	0.1003	0.0044	−0.4783	0.0049
120.0	130.9	0.5832	0.0070	0.1676	0.0053	0.0806	0.0043	−0.5187	0.0050
125.0	135.3	0.5389	0.0066	0.2886	0.0052	0.0315	0.0041	−0.5441	0.0048
130.0	139.6	0.4880	0.0062	0.3927	0.0061	−0.0552	0.0049	−0.5375	0.0054
135.0	143.8	0.4381	0.0058	0.4306	0.0059	−0.1533	0.0046	−0.5153	0.0051
140.0	148.0	0.3823	0.0053	0.4385	0.0056	−0.2273	0.0043	−0.4440	0.0048
145.0	152.2	0.3081	0.0036	0.4005	0.0037	−0.2859	0.0033	−0.3705	0.0060
150.0	156.2	0.2578	0.0049	0.3240	0.0047	−0.3109	0.0051	−0.2901	0.0054
155.0	160.3	0.1951	0.0043	0.2420	0.0061	−0.3049	0.0047	−0.1979	0.0035
160.0	164.3	0.1451	0.0037	0.1609	0.0029	−0.2731	0.0086	−0.1272	0.0031
165.0	168.2			0.0888	0.0050	−0.2157	0.0040	−0.0650	0.0039
169.7	171.9			0.0472	0.0050	−0.1532	0.0042	−0.0226	0.0042

Table 6 h. Analyzing powers of the reaction $^3He(\vec{d}, p)^4He$ at 13 MeV

θ_{lab}	θ_{cm}	iT_{11}	ΔiT_{11}	T_{20}	ΔT_{20}	T_{21}	ΔT_{21}	T_{22}	ΔT_{22}
10.0	12.2	−0.1098	0.0039	−0.7768	0.0088	0.2682	0.0047	−0.0480	0.0040
15.0	18.3	−0.2155	0.0049	−0.7358	0.0082	0.4031	0.0052	−0.1039	0.0038
20.0	24.4	−0.3720	0.0072	−0.6640	0.0055	0.5082	0.0044	−0.1948	0.0036
25.0	30.4	−0.6099	0.0091	−0.5414	0.0052	0.4559	0.0044	−0.2832	0.0061
30.0	36.4	−0.7420	0.0156	−0.3896	0.0058	0.1160	0.0041	−0.2172	0.0045
35.0	42.4	−0.5576	0.0090	−0.3252	0.0084	−0.2099	0.0030	−0.0057	0.0050
40.0	48.3	−0.3149	0.0042	−0.3196	0.0044	−0.2493	0.0034	0.1180	0.0028
45.0	54.1	−0.1858	0.0040	−0.3052	0.0038	−0.1725	0.0024	0.1499	0.0024
50.0	59.9	−0.1129	0.0035	−0.2752	0.0020	−0.0805	0.0018	0.1507	0.0013
55.0	65.6	−0.0721	0.0057	−0.2339	0.0025			0.1405	0.0024
60.0	71.2	−0.0579	0.0045	−0.1705	0.0025	0.0444	0.0024	0.1184	0.0017
65.0	76.7	−0.0319	0.0049	−0.0910	0.0021	0.0833	0.0027	0.0874	0.0026
70.0	82.1	0.0102	0.0056	0.0070	0.0029	0.0832	0.0031	0.0626	0.0030
75.0	87.5	0.0845	0.0057	0.1155	0.0028	0.0357	0.0028	0.0233	0.0028
80.0	92.7	0.2283	0.0058	0.1706	0.0040	−0.0815	0.0042	−0.0400	0.0041
85.0	97.9	0.4220	0.0069	0.1324	0.0044	−0.2009	0.0045	−0.1312	0.0045
90.0	102.9	0.6113	0.0123	−0.0110	0.0036	−0.2524	0.0036	−0.2134	0.0037
95.0	107.9	0.6888	0.0080	−0.1346	0.0058	−0.2078	0.0055	−0.2766	0.0061
100.0	112.7	0.6775	0.0067	−0.1906	0.0056	−0.1046	0.0051	−0.3345	0.0057
105.0	117.5	0.6508	0.0070	−0.1523	0.0053	−0.0193	0.0049	−0.3693	0.0055
110.0	122.1	0.6187	0.0076	−0.0737	0.0058	0.0497	0.0045	−0.4204	0.0055
115.0	126.7	0.5751	0.0073	0.0194	0.0054	0.0615	0.0043	−0.4619	0.0052
120.0	131.2	0.5356	0.0068	0.1566	0.0054	0.0586	0.0042	−0.5035	0.0051
125.0	135.6	0.5052	0.0067	0.2783	0.0053	0.0120	0.0041	−0.5218	0.0050
130.0	139.9	0.4626	0.0064	0.3706	0.0063	−0.0463	0.0050	−0.5114	0.0056
135.0	144.1	0.4254	0.0061	0.4435	0.0061	−0.1318	0.0047	−0.4813	0.0054
140.0	148.3	0.3517	0.0055	0.4586	0.0059	−0.1997	0.0046	−0.4174	0.0051
145.0	152.4	0.2928	0.0057	0.4363	0.0036	−0.2501	0.0035	−0.3343	0.0037
150.0	156.4	0.2266	0.0045	0.3724	0.0049	−0.2708	0.0054	−0.2570	0.0055
155.0	160.4	0.1737	0.0039	0.3000	0.0036	−0.2505	0.0035	−0.1675	0.0037
160.0	164.3	0.1293	0.0035	0.2307	0.0031	−0.2253	0.0059	−0.1110	0.0032
165.0	168.3			0.1718	0.0048	−0.1819	0.0040	−0.0594	0.0042
169.7	171.9			0.1339	0.0051	−0.1241	0.0042	−0.0274	0.0046

Table 7a. Normalized Legendre-polynomial coefficients $d_{11}(L) = a_{11}(L)/a_{00}(0)$ from the analysis of the analyzing power iT_{11}

E_d (MeV)	$d_{11}(1)$	$d_{11}(2)$	$d_{11}(3)$	$d_{11}(4)$	$d_{11}(5)$
1.0	−0.0379 (25)	−0.0124 (16)	−0.0058 (11)		
2.0	−0.0750 (31)	−0.0705 (19)	−0.0304 (15)	0.0013 (13)	
2.8	−0.0643 (85)	−0.0400 (55)	−0.0621 (42)	0.0067 (36)	
4.0	−0.0378 (16)	0.1298 (13)	−0.0936 (9)	0.0345 (9)	
5.0	−0.0008 (62)	0.4037 (43)	−0.0940 (39)	0.0718 (27)	−0.0059 (27)
6.0	0.0384 (22)	0.6227 (19)	−0.0756 (14)	0.0678 (12)	
8.0	0.0227 (19)	0.7681 (18)	−0.0109 (14)	0.0585 (12)	0.0180 (10)
10.0	−0.0669 (21)	0.7243 (17)	0.0351 (13)	0.0553 (12)	0.0403 (10)
11.5	−0.1054 (78)	0.6094 (59)	0.0852 (46)	0.0592 (39)	0.0546 (39)
12.0	−0.1775 (26)	0.6186 (21)	0.0583 (17)	0.0569 (16)	0.0633 (13)
13.0	−0.2107 (20)	0.5561 (17)	0.0681 (14)	0.0651 (13)	0.0749 (11)

E_d (MeV)	$d_{11}(6)$	$d_{11}(7)$	$d_{11}(8)$
5.0	−0.0020 (27)	0.0082 (23)	
8.0	0.0057 (9)		
10.0	0.0065 (9)		
11.5	0.0124 (39)	−0.0046 (33)	−0.0098 (33)
12.0	0.0100 (13)	−0.0024 (12)	0.0017 (10)
13.0	0.0159 (10)	−0.0008 (9)	0.0021 (8)

scattering plane, which changes β in the target coordinate system. In a scattering plane rotated by an angle ϕ around the beam axis z the effective value of the components of the beam polarization changes by the factor $\cos(q \cdot \beta)$,

$$\mathrm{Re}(t_{kq}(\beta)) = \cos(q \cdot \beta) \cdot \mathrm{Re}(t_{kq}(0°)), \tag{11}$$

where q refers to the corresponding index in t_{kq}. The maximum value of $\Delta\phi$ is given by the height h of the diaphragm, the distance R between target and detector, and the scattering angle θ_{lab},

$$\Delta\phi = \arctan \frac{h}{2 \cdot R \cdot \sin \theta_{\mathrm{lab}}}. \tag{12}$$

The effective polarization $\langle t_{kq} \rangle$ is obtained by the average over ϕ in the limit of $\pm \Delta\phi$,

$$\langle t_{kq} \rangle = \frac{\sin(q \cdot \Delta\phi)}{q \cdot \Delta\phi} \cdot t_{kq} = (1 - C) \cdot t_{kq}, \tag{13}$$

with C as a correction factor (cf. Table 8). No correction is required for t_{20}, since this component is independent of the azimuthal angle.

Another correction has been made for extreme scattering angles θ due to the finite height of the detectors. At forward angles this height was smaller than at larger angles. This leads to corrections smaller than the uncertainty of the angular setting of 0.1°. The corrections for the present geometry and the different observables are

Table 7 b. Normalized Legendre-polynomial coefficients $d_{20}(L) = a_{20}(L)/a_{00}(0)$ from the analysis of the analyzing power T_{20}

E_d (MeV)	$d_{20}(0)$	$d_{20}(1)$	$d_{20}(2)$	$d_{20}(3)$	$d_{20}(4)$
1.0	0.0085 (10)	−0.0986 (15)	−0.6110 (22)	0.2525 (23)	−0.0657 (28)
2.0	−0.0067 (10)	−0.2501 (16)	−0.5234 (22)	0.3853 (26)	−0.2220 (29)
2.8	−0.0108 (30)	−0.3534 (45)	−0.5359 (65)	0.2349 (76)	−0.3616 (91)
4.0	−0.0351 (14)	−0.4716 (36)	−0.6675 (54)	−0.2152 (71)	−0.6558 (75)
5.0	−0.0445 (33)	−0.5041 (62)	−0.8294 (86)	−0.4768 (111)	−0.8354 (119)
6.0	−0.0818 (12)	−0.5129 (30)	−0.8656 (44)	−0.5673 (52)	−0.8901 (56)
8.0	−0.1459 (17)	−0.5668 (45)	−0.6920 (70)	−0.6286 (86)	−0.8089 (98)
10.0	−0.1650 (15)	−0.6167 (38)	−0.4990 (59)	−0.6098 (73)	−0.5832 (81)
11.5	−0.1665 (39)	−0.6501 (78)	−0.4036 (107)	−0.5743 (143)	−0.4393 (153)
12.0	−0.1540 (9)	−0.6249 (23)	−0.3528 (35)	−0.5493 (44)	−0.3927 (50)
13.0	−0.1433 (10)	−0.6147 (27)	−0.2954 (40)	−0.5119 (51)	−0.3221 (56)

E_d (MeV)	$d_{20}(5)$	$d_{20}(6)$	$d_{20}(7)$	$d_{20}(8)$	$d_{20}(9)$
1.0	−0.0202 (31)				
2.0	−0.0602 (32)	−0.0258 (36)			
2.8	−0.1337 (100)	−0.1094 (111)	−0.0435 (117)		
4.0	−0.2081 (78)	−0.2645 (73)	−0.1419 (70)	−0.0308 (60)	−0.0114 (54)
5.0	−0.1644 (146)	−0.4255 (150)	−0.2336 (164)	−0.0517 (162)	−0.0546 (170)
6.0	−0.0201 (55)	−0.5556 (55)	−0.2210 (48)	−0.0292 (46)	
8.0	−0.0650 (98)	−0.7581 (95)	−0.2294 (84)	−0.0659 (76)	−0.0263 (60)
10.0	−0.2095 (82)	−0.8010 (78)	−0.2242 (73)	−0.0788 (67)	−0.0384 (57)
11.5	−0.3093 (176)	−0.7899 (172)	−0.2452 (185)	−0.0943 (185)	−0.0566 (192)
12.0	−0.3265 (53)	−0.7728 (51)	−0.2319 (48)	−0.0936 (45)	−0.0528 (44)
13.0	−0.3825 (60)	−0.7505 (58)	−0.2508 (56)	−0.1166 (53)	−0.0691 (49)

E_d (MeV)	$d_{20}(10)$	$d_{20}(11)$
8.0	−0.0094 (53)	
10.0	−0.0085 (46)	
12.0	−0.0144 (39)	−0.0054 (35)
13.0	−0.0198 (40)	−0.0053 (37)

collected in Table 8 for extreme angles. For the intermediate angular range the corrections are very small and are therefore neglected. These corrections are applied to the data shown in Figs. 4 to 7.

4.2.2 Spin Direction of the Beam

Systematic errors arise from the uncertainty of the spin direction after the rotation in the Wien filter. The investigation of the accuracy of the angular setting of α and β indicates that in the present measurement the maximum uncertainty is $\Delta\alpha = \Delta\beta \simeq \pm 1°$, which, according to Eqs. (7), gives an uncertainty in the T_{kq} of $\Delta T_{11} = 0.0006$,

Table 7c. Normalized Legendre-polynomial coefficients $d_{21}(L) = a_{21}(L)/a_{00}(0)$ from the analysis of the analyzing power T_{21}

E_d (MeV)	$d_{21}(1)$	$d_{21}(2)$	$d_{21}(3)$	$d_{21}(4)$	$d_{21}(5)$
1.0	0.1111 (28)	0.4802 (18)	−0.1405 (14)	0.0276 (12)	0.0042 (10)
2.0	0.2409 (24)	0.3735 (15)	−0.2334 (13)	0.0913 (11)	0.0180 (10)
2.8	0.3443 (145)	0.3528 (85)	−0.2034 (76)	0.1579 (64)	0.0321 (58)
4.0	0.3771 (23)	0.3316 (18)	0.0246 (16)	0.2661 (15)	0.0611 (14)
5.0	0.3908 (78)	0.4360 (62)	0.1307 (55)	0.3838 (47)	0.0527 (39)
6.0	0.3202 (23)	0.4082 (21)	0.1615 (19)	0.4030 (18)	0.0105 (16)
8.0	0.1795 (20)	0.3057 (18)	0.1259 (18)	0.3643 (18)	0.0085 (16)
10.0	0.0607 (14)	0.1989 (12)	0.0863 (12)	0.2746 (12)	0.0488 (12)
11.5	0.0078 (72)	0.1567 (52)	0.0618 (39)	0.2016 (39)	0.0852 (39)
12.0	−0.0141 (15)	0.1235 (13)	0.0499 (13)	0.1869 (13)	0.0842 (12)
13.0	−0.0417 (15)	0.0956 (13)	0.0336 (13)	0.1519 (13)	0.0940 (12)

E_d (MeV)	$d_{21}(6)$	$d_{21}(7)$	$d_{21}(8)$	$d_{21}(9)$	$d_{21}(10)$
2.0	0.0077 (8)	0.0017 (8)			
2.8	0.0215 (55)				
4.0	0.0670 (12)	0.0298 (11)	0.0030 (10)		
5.0	0.1229 (35)	0.0542 (39)	0.0168 (35)		
6.0	0.1538 (14)	0.0528 (12)	0.0074 (10)		
8.0	0.2010 (14)	0.0563 (13)	0.0142 (10)	0.0037 (9)	
10.0	0.2190 (10)	0.0552 (9)	0.0197 (8)	0.0076 (7)	0.0013 (6)
11.5	0.2218 (33)	0.0598 (33)	0.0241 (33)	0.0059 (33)	−0.0007 (26)
12.0	0.2105 (11)	0.0580 (9)	0.0235 (9)	0.0104 (7)	0.0024 (6)
13.0	0.1992 (11)	0.0573 (10)	0.0235 (8)	0.0112 (8)	0.0038 (7)

$\Delta T_{20} = 0.0013$, $\Delta T_{21} = 0.0073$, and $\Delta T_{22} = 0.0019$. These systematic errors are mostly smaller than the statistical errors. The T_{21} component is particularly sensitive to the orientation of the spin.

4.2.3 Switching of the Sign of the Polarization

For the determination of the observables from the detector counting rates it is assumed that the absolute values of the beam polarization are strictly equal, when the sign of the polarization is changed. Tests carried out with the beam polarization in the different modes of Table 1 show that in the worst case a difference 0.010 ± 0.005 occurs. Therefore the polarization values deviate from their mean value by less than 0.005.

4.2.4 Calibration of the Beam Polarization

Continuous monitoring of the beam polarization establishes the stability of the value of the beam polarization. Since the final polarization value is averaged over

Table 7 d. Normalized Legendre-polynomial coefficients $d_{22}(L) = a_{22}(L)/a_{00}(0)$ from the analysis of the analyzing power T_{22}

E_d (MeV)	$d_{22}(2)$	$d_{22}(3)$	$d_{22}(4)$	$d_{22}(5)$	$d_{22}(6)$
1.0	−0.2232 (10)	0.0388 (4)	−0.0045 (3)	0.0000 (2)	−0.0003 (1)
2.0	−0.1198 (9)	0.0778 (5)	−0.0149 (3)	−0.0025 (2)	−0.0017 (2)
2.8	−0.0330 (32)	0.0825 (18)	−0.0293 (13)	−0.0066 (10)	−0.0031 (8)
4.0	0.0716 (6)	0.0601 (3)	−0.0490 (2)	−0.0077 (1)	−0.0067 (1)
5.0	0.1394 (27)	0.0650 (15)	−0.0699 (10)	−0.0052 (7)	−0.0108 (5)
6.0	0.1294 (10)	0.0686 (6)	−0.0855 (4)	−0.0012 (3)	−0.0145 (2)
8.0	0.0660 (9)	0.0832 (5)	−0.0843 (3)	0.0034 (2)	−0.0181 (2)
10.0	0.0093 (8)	0.0900 (4)	−0.0661 (3)	0.0021 (2)	−0.0187 (2)
11.5	−0.0274 (42)	0.0877 (22)	−0.0567 (10)	0.0004 (9)	−0.0175 (7)
12.0	−0.0318 (7)	0.0885 (4)	−0.0479 (3)	0.0004 (2)	−0.0165 (1)
13.0	−0.0460 (5)	0.0852 (3)	−0.0398 (2)	−0.0001 (1)	−0.0147 (1)

E_d (MeV)	$d_{22}(7)$	$d_{22}(8)$	$d_{22}(9)$	$d_{22}(10)$	$d_{22}(11)$
1.0	−0.0001 (1)				
2.0	−0.0005 (1)	−0.0001 (1)			
2.8	−0.0012 (6)				
4.0	−0.0024 (1)	−0.0003 (1)			
5.0	−0.0040 (4)				
6.0	−0.0043 (2)	−0.0004 (1)			
8.0	−0.0044 (1)	−0.0010 (1)	−0.0002 (1)		
10.0	−0.0046 (1)	−0.0012 (1)	−0.0005 (1)	−0.0003 (1)	
11.5	−0.0046 (5)	−0.0012 (5)	−0.0008 (3)		
12.0	−0.0051 (1)	−0.0016 (1)	−0.0007 (1)	−0.0002 (1)	−0.0001 (1)
13.0	−0.0053 (1)	−0.0016 (1)	−0.0008 (1)	−0.0003 (1)	

Table 8. Geometrical corrections for extreme scattering angles

θ_{lab} (degree)	$\Delta\phi$ (degree)	$C(iT_{11}, T_{21})\%$	$C(T_{22})\%$	θ_{corr} (degree)
10	6.4	0.2	0.8	10.0
15	8.6	0.3	1.5	15.1
20	9.7	0.5	1.9	20.1
25	10.0	0.5	2.0	25.1
30	8.0	0.4	1.4	30.1
35	7.4	0.3	1.1	35.1
40	6.6	0.2	0.9	40.1
90	4.2	<0.1	<0.4	90.0
140	6.6	0.2	0.9	139.9
145	7.4	0.3	1.1	144.9
150	8.0	0.4	1.4	149.9
155	10.0	0.5	2.0	154.9
160	12.0	0.8	3.1	159.9
165	16.0	1.3	5.4	164.8
170	23.0	2.8	11.8	169.7

many different runs with consistent polarization values, the statistical error of the primary beam polarization is very small. Hence the absolute calibration error is determined by the calibration of the tensor analyzing power $T_{20}(E, 0°)$ of the beam polarimeter. The calibration error from ref. [2] is given as 1%. The accuracy of the polarization of the vector-polarized beam is about 2% [19]. These calibration uncertainties have to be taken into account in using the present results for deuteron polarimeters and for the comparison with model calculations.

5 Discussion and Conclusions

In the energy range between 1.0 and 13.0 MeV angular distributions of the differential cross section, the vector-analyzing power iT_{11}, and the three tensor-analyzing powers T_{20}, T_{21}, and T_{22} have been measured to a high precision. Nearly complete angular distributions, reaching from $\theta_{lab} = 10°$ to 170° (corresponding to $\theta_{cm} = 12°$ to 172°) have been obtained. The cross section is peaked in the forward direction. As the energy increases, successively one, two or three minima appear in the angular distributions first near 100°, then near 40°, and finally around 150°. The vector-analyzing power iT_{11} starts at low energy with very low values ($\leqslant 0.03$), however, quickly increases to maximum values around 0.7 with negative values at forward and positive values at backward direction, crossing the zero line near 90°. All tensor-analyzing powers on the contrary begin with large values already at low energy and, in general, an increasing complexity of the structure is observed with larger energy. Particularly the tensor component T_{21} shows a strong oscillatory behaviour at higher energy. These changes in complexity reflect the contribution of higher partial waves in the reaction under investigation.

The data have been fitted by Legendre polynomials. Excellent fits could be obtained, what reflects the quality and the consistency of the data. Increasing L-values of the Legendre polynomials have been necessary to fit the angular distributions at the higher energies.

The results show that the $^3He(d, p)^4He$ reaction is an excellent analyzer for polarized deuterons in the energy range investigated. An exception is the vector-analyzing power iT_{11} below 6 MeV. Especially the tensor-analyzing power T_{20} at small angles shows outstanding features for a polarimeter, since in this angular range also the largest cross sections occur. This is also the case for T_{21} around 30° in the energy region between 4 and 13 MeV, however, at higher energies substantial values of T_{21} occur only near a minimum of the cross section. This component has large values also near 150° for energies between 1 and 10 MeV. The oscillatory behaviour at higher energies will prevent the use of large angular detector openings in a polarimeter design. Over the whole energy range the T_{22} component shows regions with large analyzing-power values. Here the interesting regions are mostly in the backward direction.

In conclusion the present results suggest the application of this reaction for a deuteron polarimeter in the energy range of the present investigation. Since the energy behaviour is smooth, thick ^3He-targets and for most analyzing-power components also large detector solid angles are possible. These features result in a large polarimeter efficiency, which allows also the measurement of the deuteron polarization from double-scattering experiments.

References

1. Ajzenberg-Selove, F.: Nucl. Phys. **A413**, 1 (1984)
2. Dodder, D. C., Hale, G. H., Jarmie, N., Bett, J. H., Keaton Jr., P. W., Nisley, R. A., Witte, K.: Phys. Rev. **C15**, 518 (1977)
3. Plattner, G. R., Bacher, A. D., Conzett, H. E.: Phys. Rev. **C5**, 1158 (1972)
4. Schwandt, P., Clegg, T. B., Haeberli, W.: Nucl. Phys. **A163**, 432 (1971)
5. Hardekopf, R. A., Ohlsen, G. G.: Phys. Rev. **C15**, 514 (1977)
6. Houdayer, A., Davison, N. E., Elbakr, S. A., Sourkes, A. M., van Oers, W. T. H., Bacher, A. D.: Phys. Rev. **C18**, 1985 (1978)
7. Imai, K., Hatanaka, K., Shimizu, H., Tamura, N., Egawa, K., Nisimura, K., Saito, T., Sato, H., Wakuta, Y.: Nucl. Phys. **A325**, 397 (1979)
8. Saito, T.: Nucl. Phys. **A331**, 477 (1979)
9. Burzynski, S., Champbell, J., Hammans, M., Henneck, R., Lorenzon, W., Pickar, M. A., Sick, I.: Phys. Rev. **C39**, 56 (1989)
10. Ramavataram, K., Plummer, D. J., Hodges, T. A., Montague, D. G.: Nucl. Phys. **A174**, 204 (1971)
11. König, V., Grüebler, W., White, R. E., Schmelzbach, P. A., Marmier, P.: Nucl. Phys. **A185**, 263 (1972)
12. Donoghue, T. R., Ohlsen, G. G., Jarmie, N., Keaton Jr., P. W.: Phys. Rev. **C10**, 571 (1974)
13. Grüebler, W., König, V., Ruh, A., Schmelzbach, P. A., White, R. E., Marmier, P.: Nucl. Phys. **A176**, 631 (1971)
14. Silverstein, E. A.: Nucl. Instr. Meth. **4**, 53 (1955)
15. Proceedings of the 3rd International Symposium on Polarization Phenomena in Nuclear Reactions (Barschall, H. H., Haeberli, W., eds.). Madison: University of Wisconsin Press 1970
16. Singy, D., Schmelzbach, P. A., Grüebler, W., Zhang, W. Z.: Nucl. Instr. Meth. **A278**, 349 (1989)
17. Schmelzbach, P. A., Grüebler, W., König, V., Risler, R., Boerma, D. O., Jenny, B.: Nucl. Phys. **A264**, 45 (1976)
18. Grüebler, W., Schmelzbach, P. A., König, V.: Phys. Rev. **C22**, 2243 (1980)
19. Grüebler, W., Schmelzbach, P. A., König, V., Jenny, B., Risler, R., Bürgi, H. R., Nurzynski, J.: Nucl. Phys. **A271**, 29 (1976)
20. Wang, N.-M., et al.: Sov. J. Nucl. Phys. **3**, 777 (1966)

Received December 5, 1989; revised April 19, 1990; accepted for publication May 15, 1990